Hindawi
Modelling and Simulation in Engineering
Volume 2022, Article ID 7725025, 27 pages
https://doi.org/10.1155/2022/7725025

Review Article

Shear Strengthening of RC Beams with FRP Composites: Database of FE Simulations and Analysis of Studied Parameters

Amirali Abbasi, Omar Chaallal, and Georges El-Saikaly

Department of Construction Engineering, École de Technologie Supérieure (ÉTS), Université du Québec, 1100 Notre-Dame St W, (Quebec), Montreal, Canada H3C 1K3

Correspondence should be addressed to Omar Chaallal; omar.chaallal@etsmtl.ca

Received 23 May 2021; Accepted 24 November 2021; Published 21 January 2022

Academic Editor: Franco Ramírez

The use of externally bonded fiber-reinforced polymer (EB-FRP) composites for shear strengthening of reinforced concrete (RC) beams presents many challenges given the complex phenomena that come into play. Premature bond failure, the behavior of the interface layer between FRP composites and the concrete substrate, the complex and brittle nature of shear cracks, and the adverse interaction between internal steel stirrups and EB-FRP are some of these phenomena. Compared to experimental investigations, the finite element (FE) technique provides an accurate, cost-effective, and less time-consuming tool, enabling practicing engineers to perform efficient, accurate nonlinear and dynamic analysis as well as parametric studies on RC beams strengthened with EB-FRP. Since 1996, many numerical studies have been carried out on the response of RC beams strengthened using FRP. However, only a few have been related to RC beams strengthened in shear using EB-FRP composites. In addition, the analytical models that have been reported so far have failed to address and encompass all the factors affecting the contribution of EB-FRP to shear resistance because they have mostly been based on experimental studies with limited scopes. The aim of this paper is to build an extensive database of all the studies using finite element analysis (FEA) carried out on RC beams strengthened in shear with EB-FRP composites and to evaluate their strengths and weaknesses through various studied parameters.

1. Introduction

Given its complexity and its propensity to brittle failure without warning, the shear behavior of reinforced concrete (RC) beams has long been a major concern in the field of structural engineering. Therefore, practicing engineers often privilege the sequence by which flexural failure occurs before shear failure. The lack of shear resistance in RC beams can be due to various interacting factors. Underestimating the real applied loads in the design process, lack of accuracy in the construction phase, and damage due to winds and earthquakes are examples of such factors. In recent years, fiber-reinforced polymer (FRP) composites for rehabilitation and strengthening of RC beams have gained in popularity and have reached worldwide acceptance since their first use as externally bonded (EB) fabrics/laminates to strengthen existing deficient structures in the late 1990s. Their success has been due to the high strength-to-weight ratio and the tensile strength they offer, which can compensate for the shear resistance deficiency of RC beams. Researchers have investigated various FRP shapes such as fabrics, laminates, bars, and rods. However, the EB method consisting of bonding FRP fabrics/laminates to the substrate of RC beams is the most common approach. Other techniques for shear strengthening of RC beams include the embedded through-section (ETS) method as well as the near-surface (NSM) method. If the tensile strength of the concrete substrate is insufficient, mechanical anchorage systems in addition to resin epoxy are generally required. The interaction between concrete and EB-FRP composites depends on various complex interacting factors.

There have been some finite element analysis (FEA) studies of RC beams strengthened in flexure. In contrast, due to the brittle nature of shear cracks and the complex behavior of the bond between concrete and EB-FRP laminates/fabrics, very few studies have considered FEA on RC

beams strengthened in shear with EB-FRP. Because it is more cost-effective and less time-consuming than experimental studies, FEA has gained increasing attention in the last few years. Research conducted on RC beams strengthened in shear using EB-FRP has been very restricted. Some of previous studies also used simplistic assumptions, such as perfect bonding between components and a restrictive definition of shear cracks, leading to inaccurate prediction of the number and angles of shear cracks in RC beams affecting the effective bond length, further leading to inaccurate results. Finally, the other merit of FEA is that the response of all specimen components can be recorded during loading, resulting in an insightful comprehension of the complex relations between concrete, steel stirrups, longitudinal tensile reinforcement, and EB-FRP fabrics/laminates, which is impossible to attain by laboratory testing. The database built in the present study evaluates all the FEA carried out on RC beams strengthened in shear using FRP composites, including all the EB, NSM, and ETS strengthening techniques, with a special emphasis on the externally bonded method (EB). An evaluation has also been carried out on the parameters used in previous research studies as follows: type of FRP materials and shear strengthening configurations; size effect; interaction between components and types of interface element; analytical approach in FE simulations; number, size, and type of elements in simulation; ratio of EB-FRP, longitudinal, and transverse steel reinforcement; failure modes in concrete and EB-FRP (debonding, delamination, or rupture); effective stress, strain, and bond length; stress and strain distributions along the shear cracks; shape function of the crack, crack width, and crack pattern; and load-deflection response. Emphasis will be placed on showing the paramount importance of these parameters for the development of an analytical model to calculate the contribution of FRP laminates/fabrics to the ultimate shear capacity of RC beams shear-strengthened with EB-FRP.

2. Important Issues in Modeling RC Beams Strengthened with EB-FRP

To assess the crucial issues related to RC beams strengthened in shear with FRP composites, particularly their failure modes, a review of previous studies has been carried out. Among the few FE research studies related to this type of beam, only those that exhaustively described the main simulation assumptions and validated them with experimental tests were considered in this study. Modeling concrete and its cracks as an inhomogeneous material in FE models has always been a controversial issue. However, the development of FEM has paved the way for other solutions, such as implementing concrete damage plasticity theory (CDP) in the model programming. The plastic-damage model in concrete depends on the models developed by Lubliner et al. [1] and Lee and Fenves [2]. The CDP model can analyze concrete structures subjected to dynamic loading. Furthermore, it is appropriate for evaluating quasi-brittle materials like rock, mortar, and ceramics. The two main failure modes in concrete are cracking in tension and crushing in compression. The constitutive model of CDP can capture the influence of irretrievable damage related to the failure mechanisms that happen in concrete as well as in quasi-brittle materials. Modeling RC beams and their cracks on the one hand and the interaction between concrete, steel reinforcement, and FRP composites on the other are critical parts of a simulation. Generally, two models are used to describe concrete cracking: (i) the discrete crack model and (ii) the smeared crack model.

2.1. Discrete Crack Approach. The discrete crack approach depends on the geometry of the model in which crack propagation spreads among the existing borders of each element when discontinuities are defined in FE discretization. Therefore, a crack's growth and angle rely on the size and shape of the mesh in FE programs, so that this method is mesh-objective. The solution to overcome this objectivity is to define auto-remeshing programs, which lead to increased computational challenges by changing the mesh topology [3].

2.2. Smeared Crack Approach. Unlike the discrete crack model that propagates among the discontinuities in an element, the smeared crack model grows through the continuity of the material and consequently through elements, by reducing the stiffness of discretized elements. The smeared crack model can be further divided into two categories: the fixed smeared crack model and the rotated smeared crack model. The former model does not change the crack angle, and as the load increases, a crack propagates during the whole calculation process. In the rotated smeared crack model, on the other hand, the orientation of the crack changes as the load increases, and new orientations are determined based on directions of updated main stresses and strains. Nevertheless, the smeared crack method leads to localization of strain, which means that when the element dimension is close to zero, the energy consumption approaches zero. This issue was solved by introducing the crack band model, which links the fracture energy to the constitutive law of concrete. Therefore, the fracture energy during crack propagation does not rely on the dimension of the element and the mesh, making this technique not mesh-objective [3].

2.3. Interactions between Steel Reinforcement and Concrete. Studies conducted by previous researchers have shown that there is an inverse interaction between EB-FRP and steel reinforcement, particularly steel stirrups, which means that when the number of steel stirrups increases, the contribution of EB-FRP to shear resistance decreases [4]. Furthermore, it has been shown that assuming a perfect bond model between the longitudinal steel reinforcement and the concrete results in more distributed crack patterns, leading to a narrower crack width. This affects the debonding process, which occurs in a later stage than without the assumption and consequently overestimates the ultimate shear resistance of the beam [3]. However, noticeable disparities have been observed on the overall load-displacement curves of the specimens. The bond-slip model introduced in the European CEB-FIP Model Code 1990 [5] is an appropriate indication of interaction between the concrete and the steel reinforcement [3].

2.4. Interface between EB-FRP and Concrete. To predict the ultimate shear capacity of RC beams strengthened in shear using EB-FRP, the interaction between concrete and FRP composites should be defined precisely, because otherwise debonding mechanism between concrete and FRP composites cannot be detected. In addition, an accurate definition of the concrete-FRP interaction affects the angle and distribution of shear cracks. Indeed, the assumption of perfect bonding results in distributed diagonal shear cracks, whereas the correct bond model definition leads to one main diagonal shear crack. Therefore, assuming a perfect bond model between concrete and EB-FRP composites overestimates the ultimate load-carrying capacity of the beam [3]. This demonstrates the importance of defining the bond model between concrete and FRP composites with high precision and accuracy.

3. Review and Synthesis of Previous Work on FE Modeling

When FRP composites were introduced in the construction industry, computer programs and FE packages were not developed as much as today. As a result, most evaluations of the efficiency of RC beams strengthened in shear with EB-FRP composites were based on laboratory tests, and hence, the effect of many parameters on the overall response of these tested beams could not be detected. This was particularly true when some of these parameters interacted with each other, making the behavior of these beams complex and difficult to fully understand. In addition, once FE programs were developed, most studies that used them concentrated on strengthening in flexure of RC beams using EB-FRP composites. In this section, the main FE studies carried out on RC beams strengthened in shear, as well as the major parameters affecting the response of these beams and their components, are gathered and presented in Figure 1.

Figure 1 includes 37 studies from 1996 to 2020, with a total of 239 RC beams strengthened in shear using FRP composites; six of them were subjected to microscopic studies in which the stress and strain distributions along fictional diagonal shear cracks and the effective bond length were examined [6, 7], and the rest (233 beams) were simulated using FE software. The details of these 239 shear-strengthened RC beams subjected to FEA are presented in Tables 1–3. Generally, in terms of depth, RC beams are generally classified into three groups depending on their shear span-to-depth ratio (a/d) as follows: (i) a/d less than 1 is a deep beam; (ii) a/d between 1 and 2.5 is a moderately deep beam, with shear failure likely occurring before flexure failure; and (iii) a/d equal to or greater than 2.5 is a flexural slender beam that often exhibits flexure before shear failure.

The shape of RC beams is designed based on their applications and the load they carry. For example, beams with an I cross section are generally used by the road and bridge construction industries in which shear strength is of paramount importance, whereas beams with a T cross section can be designed for either the road building or the housing industry. Figure 2 presents a histogram of 233 RC beams strengthened in shear using EB-FRP and studied by FEA to evaluate the shear contribution of FRP to the ultimate shear capacity of beams. The histogram shows that, among the 233 beams, 46 were T-shaped, 175 were rectangular, and 12 were I-shaped cross sections, representing 19.7%, 75.1%, and 5.1%, respectively, of all the shear-strengthened RC beams. Therefore, despite their generalized use in practice, few FE studies focused on T cross-sectional beams (19.7%), indicating the need for more research on the response of these beams and their influencing parameters. Shear span-to-depth ratio plays a crucial role in the behavior of these beams, and, as illustrated in the histogram, 110 (47.2%) and 118 (52.9%) of the beams belong to the moderately deep ($1 < a/d < 2.5$) and the flexural slender ($a/d \geq 2.5$) beam categories, respectively, showing that more research is needed on deep beams ($a/d \leq 1$) where shear failure usually occurs before flexure failure.

The configuration type of shear strengthening using EB-FRP is to some extent a function of the cross section of RC beams. For instance, the full-wrap technique cannot be used for shear strengthening of T-shaped or I-shaped section beams because the flange of these beams is generally not accessible. To this end, other effective methods of shear strengthening can be used for these beam cross section shapes, such as side-bonded, U-shaped, ETS, or NSM techniques. As for the interaction between stirrups and FRP composites, experimental tests show that the ETS configuration leads to a greater contribution to shear resistance compared to EB-FRP. In addition, because the concrete core is generally stronger than its surface, more confinement is expected on the ETS bond than with externally bonded (EB) methods. Simple installation and high efficiency are some of the merits of this method. Among the 239 RC beams of all studies presented in Figures 1, 221 (92%) beams were subjected to FE studies that focused on shear strengthening using the EB method (side-bonded, U-wrap, and full-wrap EB-FRP configurations) (Table 1), and only 18 (8%) beams corresponded to the ETS and NSM methods (Table 2). In addition, as illustrated in Figure 3, among the 239 RC beams shear-strengthened with FRP, only 39 beams (16.3%) were T-shaped cross sections, indicating the research needs for FEA to study the parameters affecting the response of such beams.

4. Main Studied Parameters Using FEA of Shear-Strengthened Beams

With the advantages of FEA, many of the shear responses of RC beams strengthened using FRP composites that cannot be captured by experiments can be studied from initiation of loading to ultimate failure while recording the whole failure process and its mechanisms. Most of the results derived from laboratory tests were based on the load-deflection response of the beam and the strain on the FRP composite obtained from strain gauges installed on FRP laminates, fabrics, and bars. In contrast, more parameters can be observed and studied using FEA, as illustrated in Figure 4, which highlights the variations in all components of the shear-strengthened beams. In addition, the complex interactive behavior between the components (concrete, longitudinal steel reinforcement, steel stirrups, and FRP composite) of

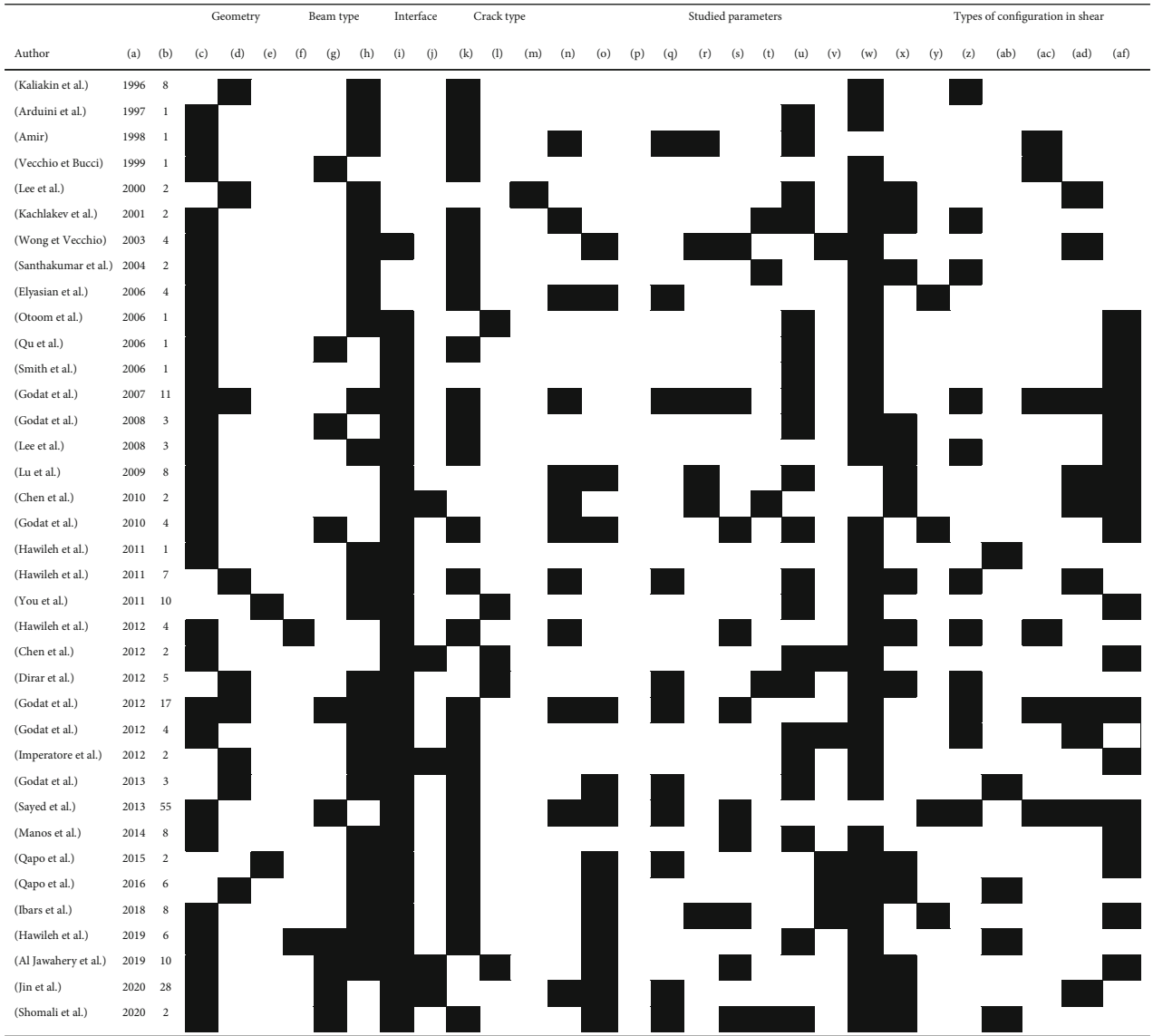

Figure 1: Summary of parameters studied on RC beams strengthened in shear by FRP composites by FEA. Note: (a) year; (b) no. of specimens; (c) rectangular section; (d) T-section; (e) I-section; (f) $a/d \leq 1$; (g) $1 < a/d < 2.5$; (h) $a/d \geq 2.5$; (i) interface (concrete-to-FRP); (j) interface (concrete-to-steel); (k) smeared crack model; (l) smeared + crack band; (m) discrete crack model; (n) types of configuration in shear and different FRP materials; (o) size effect, concrete strength; (p) analysis approach types of solvers in FEA (dynamic versus static); (q) ratio of longitudinal steel reinforcements ρ_w, steel stirrups ρ_s, and EB FRP ρ_{FRP}; (r) effective stress and strain, bond-length, distribution factors; (s) types of the failure (debonding, delamination, rapture); (t) number, size, types of elements in simulation; (u) strain, stress and slip distribution along the vertical, horizontal axis of the beam or along diagonal crack on FRP fabrics/laminates; (v) interaction between components, types of interface elements; (w) load-deflection curve, total shear capacity, (x) shape function of the crack, crack pattern, crack width; (y) full wrap; (z) continuous U wrap; (ab) NSM, ETS; (ac) continuous side-bonded; (ad) side-bonded strips; (af) U strips.

the studied beams and their interrelations can be interpreted to achieve a more precise closed-form model that integrates all these factors.

4.1. Shape Function of the Crack, Crack Pattern, and Crack Width. Because the width of a crack along its propagation path is not constant, the strain and stress distributions on FRP laminates/fabrics are not uniform. This nonuniformity of stresses and strains influences the response of steel stirrups and FRP laminates/fabrics. This means that the steel stirrups crossed by the shear crack reach the yielding point, and then, the FRP laminates/fabrics crossed by the shear cracks reach their maximum tensile strength, leading to rupture. Therefore, Chen and Teng [8] introduced a distribution factor to calculate the effective stress and strain in FRP laminates/fabrics:

$$f_{FRP,e} = D_{FRP} \times f_{FRP}, \tag{1}$$

where D_{FRP} is the distribution factor, which is function of

Table 1: Database of numerical studies assessing parameters of RC beams strengthened in shear with externally bonded FRP composites and validating with and without experimental tests.

Specimen	Section	d_{fv}	h_f	h_w	b_w	d	nt_f	a/d	f'_c	ρ_{FRP}(%)	ρ_w(%)	ρ_s(%)	Configuration	β(degree)	Fiber	E_s	E_{FRP}	ε_{fu}	$V_{t\{exp\}}$	$V_{t(NUM)}$
Kaliakin et al. [25]																				
C1	T	88.9	63.5	127	63.5	152.4	—	2.67	59.6	0	2.05	0	—	—	—	200	—	—	38.3	37.7
C2	T	88.9	63.5	127	63.5	152.4	—	2.67	74.3	0	2.05	0	—	—	—	200	—	—	39.8	39.3
C3	T	88.9	63.5	127	63.5	152.4	—	2.67	54.5	0	2.05	0	—	—	—	200	—	—	38.5	38
C4	T	88.9	63.5	127	63.5	152.4	—	2.67	56.5	0	2.05	0	—	—	—	200	—	—	36	35.5
A1	T	88.9	63.5	127	63.5	152.4	1.04	2.67	54.5	3.28	2.05	0	CT-U	90	A	200	11.03	0.0225	77.4	78.4
A2	T	88.9	63.5	127	63.5	152.4	1.04	2.67	58.0	3.28	2.05	0	CT-U	90	A	200	11.031	0.0225	60.1	—
E1	T	88.9	63.5	127	63.5	152.4	0.46	2.67	50.2	1.44	2.05	0	CT-U	90	E-G	200	14.27	0.0134	73.5	—
E2	T	88.9	63.5	127	63.5	152.4	0.46	2.67	58.0	1.44	2.05	0	CT-U	90	E-G	200	14.27	0.0134	67.9	61.5
G1	T	88.9	63.5	127	63.5	152.4	0.58	2.67	52.7	1.833071	2.05	0	CT-U	90	G	200	20.96	0.0095	71	64.3
G2	T	88.9	63.5	127	63.5	152.4	0.58	2.67	56.6	1.833071	2.05	0	CT-U	90	G	200	20.960	0.0095	72.9	66
45G1	T	88.9	63.5	127	63.5	152.4	0.58	2.67	56.6	1.833071	2.05	0	CT-U	45	G	200	20.960	0.0095	75.1	68
45G2	T	88.9	63.5	127	63.5	152.4	0.58	2.67	50.2	1.833071	2.05	0	CT-U	45	G	200	20.960	0.0095	94.5	85.6
Arduini et al. [26]																				
B4	R	350	—	400	300	350	0.51	3.14	39.6	0.113333	0.37	0.28	CT-U	90	C	200	400	0.0075	—	—
Amir [27]																				
IF	R	175	—	200	127	175	2	2.61	36.5	3.149606	1.80	0.21	CTS	45	C	200	34.13	—	—	—
Vecchio and Bucci [28]																				
Beam 1	R	935	—	1000	550	935	—	2.16	44.7	—	0.81	0.06	—	—	—	492	—	—	1700	1800
Beam 2	R	935	—	1000	550	935	1	2.16	44.7	0.363636	0.81	0.06	CTS	90	C	492	230	0.0142	2528	—
Lee et al. [29]																				
Model 1	T	192.8	75	230	140	267.8	—	2.98	25	—	4.46	0.18	—	—	—	200	—	—	—	64
Model 2	T	192.8	75	230	140	267.8	—	2.98	25	—	4.46	0.18	—	—	—	200	—	—	—	48
Model 3	T	192.8	75	230	140	267.8	1.2	2.98	25	0.337458	4.46	0.18	ST-U	90	C	200	165	0.014	—	78
Model 4	T	192.8	75	230	140	267.8	1.2	2.98	25	0.337458	4.46	0.18	ST-U	90	C	200	165	0.014	—	93
Kachlakev et al. [30]																				
Control beam	R	—	—	768.35	305	704.85		2.59	16.7	0	0.54	0	—	—	—	200	—	—	476	454
Shear beam	R	679.45	—	768.35	305	704.85	5.2	2.59	14.7	3.409836	0.54	0	CTS	90	Glass	200	21	—	689	525
Flexure/shear beam	R	679.45	—	768.35	305	704.85	5.2	2.59	13.0	3.409836	0.54	0	CTS + flexural strengthening	90	C/ glass	200	62-21	—	712	930
Wong and Vecchio [31]																				
RWOA-1	R	470	—	560	305	470	0.84	3.89	22.6	0.367213	1.67	—	ST-S	90	C	217.87	72.4	0.011	493	—
RWOA-2	R	470	—	560	305	470	0.84	4.86	25.9	0.367213	2.16	—	ST-S	90	C	217.87	72.4	0.011	457	—
RWOA-3	R	470	—	560	305	470	0.84	6.80	43.5	0.367213	2.65	—	ST-S	90	C	205.46	72.4	0.011	436	—
Beam 1 (De rose)	R	935	—	560	550	935		2.16	44.7	—	0.81	0.06	—	—	—	492	—	—	1700	1800
Beam 2 (De rose)	R	935	—	560	550	935	1	2.16	44.7	0.363636	0.81	0.06	CTS	90	C	492	230	0.0142	2528	2465
Santhakumar et al. [32]																				
C48	R	164.05	—	203.2	127	164.05	—	2.78	36.5	—	1.93	0.21	—	—	—	200	—	—	—	—
IIIFu	R	164.05	—	203.2	127	164.05	1.49	2.78	36.5	2.36063	1.93	0.21	CT-U	45	C	200	28.3	0.009	—	—
IE	R	164.05	—	203.2	127	164.05	2.18	2.78	36.5	3.43937	1.93	0.21	CT-U	90	C	200	34.1	0.009	—	—

Table 1: Continued.

Specimen	Section	d_{fv}	h_f	h_w	b_w	d	nt_f	a/d	f'_c	ρ_{FRP}(%)	ρ_w(%)	ρ_s(%)	Configuration	β(degree)	Fiber	E_s	E_{FRP}	ε_{fu}	$V_{t(\exp)}$	$V_{t(NUM)}$
Elyasian et al. [33]																				
SB-90	R	320.5	—	380	230	320.5	0.18	2.85	31	0.156522	1.33	0.18	CTW	90	C	200	228	0.018	451	—
SB-90-0	R	320.5	—	380	230	320.5	0.36	2.85	31	0.313043	1.33	0.18	CTW	90	C	200	228	0.018	468	—
SB-45	R	320.5	—	380	230	320.5	0.18	2.85	31	0.156522	1.33	0.18	CTW	45	C	200	228	0.018	529	—
SB-45-0	R	320.5	—	380	230	320.5	0.36	2.85	31	0.313043	1.33	0.18	CTW	45	C	200	228	0.018	528	—
Otoom et al. [34]																				
S03-1	R	260	—	305	150	260		2.92	28	—	4.12	—	—	—		200	—	—	154	—
S03-2	R	260	—	305	150	260	0.16	2.92	28	0.088	4.12	—	ST-U	90	C	200	228	0.0165	262	265
Qu et al. [35]																				
S0-2-0	R	260	—	—	—	260	—	2.15	31.8	—	2.9	0.19	—	0	—	—	—	—	—	—
S-CU-2-1	R	260	—	—	—	260	—	2.15	37.6	0.074	2.9	0.19	ST-U	90	C	—	235	—	—	—
Smith et al. [36]																				
BS3	—	—	—	—	—	—	—	—	—	—	—	—	—	—	—	—	—	—	—	—
BS5	—	—	—	—	—	—	—	—	—	—	—	—	ST-U	—	—	—	—	—	—	—
Godat et al. [37]																				
B-1	R	—	—	200	150	170		3	30.5	—	2.98	—	—	—	—	182	—	—	40	41
B-8	R	170	—	200	150	170	0.16	3	35.4	0.222667	2.98	—	CT-U	90	C	182	230	0.015	86	90
TR30D1	R	250	—	300	150	250		3	31.4	—	—	0.33	—	—	—	210	—	—	322	323
TR30D3	R	250	—	300	150	250	0.16	3	31.4	0.22	—	0.33	CTS	90	C	210	233.6	0.015	323	336
TR30D4	R	250	—	300	150	250	0.33	3	31.4	0.44	—	0.33	CTS	90	C	210	233.6	0.015	400	399
TR30D2	R	250	—	300	150	250	0.49	3	31.4	0.66	—	0.33	CTS	90	C	210	233.6	0.015	422	414
BT1	T	256.66	100	305	150	356.66	—	3	35	—	2.30	—	—	—	—	200	—	—	178	184
BT2	T	256.66	100	305	150	356.66	0.16	3	35	0.22	2.30	—	CT-U	90	C	200	228	0.0166	309	313
BT3	T	256.66	100	305	150	356.66	0.33	3	35	0.44	2.30	—	CT-U	90	C	200	228	0.0166	310	313
BT4	T	256.66	100	305	150	356.66	0.16	3	35	0.088	2.30	—	ST-U	90	C	200	228	0.0166	324	325
BT5	T	256.66	100	305	150	356.66	0.16	3	35	0.088	2.30	—	ST-S	90	C	200	228	0.0166	243	247
BT6	T	256.66	100	305	150	356.66	0.16	3	35	0.22	2.30	—	CT-U + anchorage	90	C	200	228	0.0166	442	453
US	R	216	—	250	150	216		2.5	35	—	—	—	—	—	—	200	—	—	114	119
RS90	R	216	—	250	150	216	1	2.5	35	0.666667	—	—	ST-S	90	C	200	150	0.014	184	197
RS135	R	216	—	250	150	216	1	2.5	35	0.444444	—	—	Inclined ST-S	45	C	200	150	0.014	194	202
Godat et al. [38]																				
RC1	R	—	—	200	100	166		2.04	51.2	—	4.1	—	—	90	—	200	235	—	160	166
U4	R	166	—	200	100	166	0.111	2.04	51.2	0.1332	4.1	—	ST-U	90	C	200	235	0.0151	203	213
RC2	R	—	—	400	200	330		2.06	49.7	—	4.5	—	—	90	—	200	235	—	709	745
U5	R	330	—	400	200	330	0.222	2.06	51.2	0.1332	4.5	—	ST-U	90	C	200	235	0.0151	809	813
RC3	R	—	—	600	300	498		2.04	50.5	—	4.2	—	—	90	—	200	235	—	1626	1659
U6	R	498	—	600	300	498	0.33	2.04	51	0.1332	4.2	—	ST-U	90	C	200	235	0.0151	2018	2053
Lee et al. [39]																				
SO3-1	R	253.33	—	305	150	253.33		3	27.5	—	4.23	—	—	90	—	200	—	—	154	—
SO3-2	R	253.33	—	305	150	253.33	0.16	3	27.5	0.088	4.23	—	ST-U	90	C	200	228	0.0166	262	—
SO3-4	R	253.33	—	305	150	253.33	0.16	3	27.5	0.22	4.23	—	CT-U	90	C	200	228	0.0166	289	—
SO3-5	R	253.33	—	305	150	253.33	0.33	3	27.5	0.44	4.23	—	CT-U	90	C	200	228	0.0166	339	—

Table 1: Continued.

Specimen	Section	d_{fv}	h_f	h_w	b_w	d	nt_f	a/d	f'_c	ρ_{FRP}(%)	ρ_w(%)	ρ_s(%)	Configuration	β(degree)	Fiber	E_s	E_{FRP}	ε_{fu}	$V_{t(exp)}$	$V_{t(NUM)}$
Godat et al. [40]																				
RC1	R	—	—	200	100	166		2.04	51.2	—	4.1	—	—	90	—	200	235	—	160	166
U4	R	166	—	200	100	166	0.11	2.04	51.2	0.1332	4.1	—	ST-U	90	C	200	235	0.0151	203	213
RC2	R		—	400	200	330		2.06	49.7	—	4.5	—	—	90	—	200	235	—	709	745
U5	R	330	—	400	200	330	0.22	2.06	51.2	0.1332	4.5	—	ST-U	90	C	200	235	0.0151	809	813
RC3	R	—	—	600	300	498		2.04	50.5	—	4.2	—	—	90	—	200	235	—	1626	1659
U6	R	498	—	600	300	498	0.33	2.04	51	0.1332	4.2	—	ST-U	90	C	200	235	0.0151	2018	2053
W7	R	498	—	600	300	498	0.33	2.04	51	0.222	4.2	—	CTW	90	C	200	235	0.0151	2221	2203
You et al. [41]																				
T4-12-control	I	817	—	—	152	944	—	2.9	68.5	0	—	0.31	—	—	—	178	210	—	894	903
T4-18-control	I	817	—	—	152	944	—	2.9	68.7	0	—	0.2	—	—	—	178	210	—	912	858
T4-18-S90-NA	I	817	—	—	152	944	0.31	2.9	69.1	0.14	—	0.2	ST-U	90	C	178	210	0.017	983	961
T4-18-S90-CMA	I	817	—	—	152	944	0.31	2.9	69.8	0.14	—	0.2	ST-U	90	C	178	210	0.017	1085	1010
T4-18-S90-DMA	I	817	—	—	152	944	0.31	2.9	70	0.14	—	0.2	ST-U	90	C	178	210	0.017	1005	1023
T4-12-control-deck	I	817	—	—	152	944	—	2.9	73.5	0	—	0.31	—	—	—	178	210	—	1090	1112
T4-12-S90-SDMA	I	817	—	—	152	944	0.31	2.9	71.2	0.14	—	0.31	ST-U	90	C	178	210	0.017	1139	1174
T3-12-control	I	655	—	—	152	782	—	3.4	61.3	0	—	0.31	—	—	—	178	210	—	1121	1014
T3-12-S90-NA	I	655	—	—	152	782	0.31	3.4	61.4	0.14	—	0.31	ST-U	90	C	178	210	0.017	1201	1152
T3-12-S90-NA-PC	I	655	—	—	152	782	0.31	3.4	65.3	0.14	—	0.31	ST-U	90	C	178	210	0.017	1085	1143
T3-12-S90-DMA	I	655	—	—	152	782	0.31	3.4	71.6	0.14	—	0.31	ST-U	90	C	178	210	0.017	1108	1143
T3-18-control	I	655	—	—	152	782	—	3.4	66.1	0	—	0.2	—	—	—	178	210	—	1121	912
T3-18-S90-NA	I	655	—	—	152	782	0.31	3.4	69.8	0.14	—	0.2	ST-U	90	C	178	210	0.017	943	907
T3-18-S90-HS	I	655	—	—	152	782	0.31	3.4	70.2	0.14	—	0.2	ST-U	90	C	178	210	0.017	979	894
T3-18-S90-SDMA	I	655	—	—	152	782	0.31	3.4	71.9	0.14	—	0.2	ST-U	90	C	178	210	0.017	1045	907
Hawileh et al. [42]																				
TB 1-60-90°	T	260	120	75	285	335	0.12	5	32.4	0.1666	0.98	0	ST-S	90	C	205	231	0.017	57.17	55.07
TB 1-0-90°	T	260	120	75	285	335	0.12	5	32.4	0.2	0.98	0	CT-S	90	C	205	231	0.017	—	65.13
TB 1-17-90°	T	260	120	75	285	335	0.12	5	32.4	0.58	0.98	0	ST-S	90	C	205	231	0.017	—	60
TB 1-153-90°	T	260	120	75	285	335	0.12	5	32.4	0.06	0.98	0	ST-S	90	C	205	231	0.017	—	47
TB 2-60-90°	T	260	120	75	285	335	0.24	5	32.4	0.333	0.98	0	ST-S	90	C	205	231	0.017	—	58
TB 3-60-90°	T	260	120	75	285	335	0.36	5	32.4	0.5	0.98	0	ST-S	90	C	205	231	0.017	—	63
TB 1-60-45° X	T	260	120	75	285	335	0.12	5	32.4	0.166	0.98	0	Inclined ST-S	45	C	205	231	0.017	—	65
Hawileh et al. [43]																				
FS-200-C	R	400	—	80	500	400	0.381	0.8	21	0.95	1.54	0.46	CT-U	90/0	C	200	230	0.015	270.5	270
FS-250-C	R	400	—	80	500	400	0.381	0.8	21	0.95	1.54	0.46	CT-U	90/0	C	200	230	0.015	182	186
FS-250-T	R	400	—	80	500	400	0.381	0.8	21	0.95	1.54	0.46	CT-U	90/0	C	200	230	0.015	219.4	219.3
FS-250-B	R	400	—	80	500	400	0.381	0.8	21	0.95	1.54	0.46	CT-U	90/0	C	200	230	0.015	186.6	185.5

Table 1: Continued.

Specimen	Section	d_{fv}	h_f	h_w	b_w	d	nt_f	a/d	f'_c	ρ_{FRP}(%)	ρ_w(%)	ρ_s(%)	Configuration	β(degree)	Fiber	E_s	E_{FRP}	ε_{fu}	$V_{t\{exp\}}$	$V_{t(NUM)}$
Chen et al. [3]																				
SO3-1	R	260	—	305	150	260	—	2.92	27.5	—	4.12	—	—	—	—	200	—	—	154	—
SO3-2	R	260	—	305	150	260	0.16	2.92	27.5	0.088	4.12	—	ST-U	90	C	200	228	0.0166	262	—
BS3	R	403.22	—	450	200	403.22	—	3.1	37.5	—	2.33	0.07	—	—	—	200	—	—	136.6	—
BS5	R	403.22	—	450	200	403.22	0.11	3.1	36	0.013875	2.33	0.07	ST-U	90	C	200	233	0.015	170	—
Dirar et al. [44]																				
F/295/LP1/4.5	T	295	105	245	105	295	0.39	3.8	24	0.249524	4.5	0.21	CT-U	90	C	200	238	0.018	135	114.8-134.4-134.4
F/295/LP2/4.5	T	295	105	245	105	295	0.39	3.8	27	0.249524	4.5	0.21	CT-U	90	C	200	238	0.018	133.5	127.2-153.6-142.4
F/215/LP1/4.6	T	215	105	165	105	215	0.39	3.8	32	0.249524	4.6	0.21	CT-U	90	C	200	238	0.018	122.5	113-132.6-132.4
F/215/LP2/4.6	T	215	105	165	105	215	0.39	3.8	25	0.249524	4.6	0.21	CT-U	90	C	200	238	0.018	102.5	96.6-115.6-109
F/295/LP1/3.3	T	295	105	245	105	295	0.39	3.8	28	0.249524	3.3	0.21	CT-U	90	C	200	238	0.018	96.5	125-108-119
Godat et al. [45]																				
SGU-1-1	R	—	—	—	150	—	—	1.5	—	—	—	—	—	—	—	—	—	—	355	368
S0-2-0	R	—	—	—	150	—	—	1.5	—	—	—	—	—	—	—	—	—	—	222	230
SGU-2-1a	R	—	—	—	150	—	—	1.5	—	—	—	—	—	—	—	—	—	—	301	300
SGU-2-1b	R	—	—	—	150	—	—	1.5	—	—	—	—	—	—	—	—	—	—	516	515
SGU-2-2	R	—	—	—	150	—	—	2.15	—	—	—	—	—	—	—	—	—	—	285	301
SGU-2-3	R	—	—	—	150	—	—	2.15	—	—	—	—	—	—	—	—	—	—	347	366
SCU-2-1	R	—	—	—	150	—	—	2.15	—	—	—	—	—	—	—	—	—	—	294	291
SGO-2-1	R	—	—	—	150	—	—	2.15	—	—	—	—	—	—	—	—	—	—	530	538
SGUB-2-1	R	—	—	—	150	—	—	2.8	—	—	—	—	—	—	—	—	—	—	306	314
SGU-3-1	R	—	—	—	150	—	—	2.8	—	—	—	—	—	—	—	—	—	—	221	239
R1	T	—	—	—	225	—	—	2.8	—	—	—	—	—	—	—	—	—	—	495	515
0.75D	T	—	—	—	225	—	—	3	—	—	—	—	ST-U	—	—	—	—	—	762	804
0.6D	T	—	—	—	225	—	—	3	—	—	—	—	ST-U	—	—	—	—	—	797	816
0.5D	T	—	—	—	225	—	—	3	—	—	—	—	ST-U	—	—	—	—	—	892	940
RC1	R	166	—	200	100	166	—	2.04	51.2	—	4.1	—	—	90	—	200	235	—	160	166
U4	R	166	—	200	100	166	0.11	2.04	51.2	0.1332	4.1	—	ST-U	90	C	200	235	0.0151	203	213
RC2	R	330	—	400	200	330	—	2.06	49.7	—	4.5	—	—	90	—	200	235	—	709	745
U5	R	330	—	400	200	330	0.22	2.06	51.2	0.1332	4.5	—	ST-U	90	C	200	235	0.0151	809	813
RC3	R	498	—	600	300	498	—	2.04	50.5	—	4.2	—	—	90	—	200	235	—	1626	1659
U6	R	498	—	600	300	498	0.33	2.04	51	0.1332	4.2	—	ST-U	90	C	200	235	0.0151	2018	2050
W7	R	498	—	600	300	498	—	3	—	—	—	—	—	—	—	—	—	0.0151	2221	2203
B-1	R	170	—	200	150	170	—	3	30.5	—	2.98	—	—	—	—	182	—	—	40	41
B-8	R	170	—	200	150	170	0.16	3	35.4	0.222667	2.98	—	CT-U	90	C	182	230	0.015	86	90
TR30D1	R	250	—	300	150	250		3	31.4	—	—	0.33	—	—	—	210	—	—	322	323
TR30D3	R	250	—	300	150	250	0.16	3	31.4	0.22	—	0.33	CTS	90	C	210	233.6	0.015	323	336
TR30D4	R	250	—	300	150	250	0.33	3	31.4	0.44	—	0.33	CTS	90	C	210	233.6	0.015	400	399
TR30D2	R	250	—	300	150	250	0.49	3	31.4	0.66	—	0.33	CTS	90	C	210	233.6	0.015	422	414
BT1	T	256.66	100	305	150	356.66		3	35	—	2.30	—	—	—	—	200	—	—	178	184
BT2	T	256.66	100	305	150	356.66	0.16	3	35	0.22	2.30	—	CT-U	90	C	200	228	0.0166	309	313

Table 1: Continued.

Specimen	Section	d_{fv}	h_f	h_w	b_w	d	nt_f	a/d	f'_c	ρ_{FRP}(%)	ρ_w(%)	ρ_s(%)	Configuration	β(degree)	Fiber	E_s	E_{FRP}	ε_{fu}	$V_{t(\exp)}$	$V_{t(NUM)}$
BT3	T	256.66	100	305	150	356.66	0.33	3	35	0.44	2.30	—	CT-U	90	C	200	228	0.0166	310	313
BT4	T	256.66	100	305	150	356.66	0.16	3	35	0.088	2.30	—	ST-U	90	C	200	228	0.0166	324	325
BT5	T	256.66	100	305	150	356.66	0.16	3	35	0.088	2.30	—	ST-S	90	C	200	228	0.0166	243	247
BT6	T	256.66	100	305	150	356.66	0.16	3	35	0.22	2.30	—	CT-U + anchorage	90	C	200	228	0.0166	442	453
US	R	216	—	250	150	216		2.5	35	—	1.63	0.21	—	—	—	200	—	—	114	119
RS90	R	216	—	250	150	216	1	2.5	35	0.666667	1.63	0.21	ST-S	90	C	200	150	0.014	184	197
RS135	R	216	—	250	150	216	1	2.5	35	0.444444	1.63	0.21	Inclined ST-S	45	C	200	150	0.014	194	202
Godat et al. [46]																				
B-1	R	170	—	200	150	170	—	3	30.5	—	2.98	—	—	—	—	182	—	—	80	82-82
B-8	R	170	—	200	150	170	0.16	3	35.4	0.222667	2.98	—	CT-U	90	C	182	230	0.015	172	180-159
TR30D1	R	250	—	300	150	250	—	3	31.4	—	—	0.33	—	—	—	210	—	—	322	323-323
TR30D3	R	250	—	300	150	250	0.16	3	31.4	0.22	—	0.33	ST-S	90	C	210	233.6	0.015	323	336-300
US	R	216	—	250	150	216	—	2.5	35	—	1.63	0.21	—	—	—	200	—	—	114	119-119
RS90	R	216	—	250	150	216	1	2.5	35	0.666667	1.63	0.21	ST-S	90	C	200	150	0.014	184	162-176
RS135	R	216	—	250	150	216	1	2.5	35	0.444444	1.63	0.21	Inclined ST-S	45	C	200	150	0.014	194	202-184
Imperatore et al. [47]																				
TM1	T	273	210	315	260	483	—	—	19.1	—	0.72	0.15	ST-U	45	C	—	65.5	0.00822	450	—
TM2	T	268	210	310	260	478	—	—	25.5	—	0.72	0.15	ST-U	45	C	—	65.5	0.00822	500	—
Sayed et al. [48]																				
2S-1	R	360	—	400	200	360	0.1	1.8	30	0.05	2.05	0.25	ST-S	90	C	240	200	0.015	—	163.1
2S-2	R	360	—	400	200	360	0.2	1.8	30	0.1	2.05	0.25	ST-S	90	C	240	200	0.015	—	174.3
2S-3	R	360	—	400	200	360	0.3	1.8	30	0.15	2.05	0.25	ST-S	90	C	240	200	0.015	—	180.8
2S-4	R	360	—	400	200	360	0.2	1.8	30	0.066667	2.05	0.25	ST-S	90	C	240	200	0.015	—	163.0
2S-5	R	360	—	400	200	360	0.2	1.8	30	0.05	2.05	0.25	ST-S	90	C	240	200	0.015	—	152.3
2S-6	R	360	—	400	200	360	0.2	1.8	30	0.2	2.05	0.25	CT-S	90	C	240	200	0.015	—	218.8
2S-7	R	360	—	400	200	360	0.2	1.8	30	0.1	2.05	0.25	ST-S	90	C	240	200	0.015	—	162.9
2S-8	R	360	—	400	200	360	0.2	1.8	30	0.1	2.05	0.25	ST-S	90	C	240	200	0.015	—	178.8
2S-9	R	360	—	400	200	360	0.2	1.5	30	0.1	2.05	0.25	ST-S	90	C	240	200	0.015	—	178.7
2S-10	R	360	—	400	200	360	0.2	2.25	30	0.1	2.05	0.25	ST-S	90	C	240	200	0.015	—	172.9
2S-11	R	360	—	400	200	360	0.2	1.8	30	0.333333	2.05	0.25	CT-S	90	C	240	200	0.015	—	198.3
2S-12	R	360	—	400	200	360	0.2	1.8	30	0.1	2.05	0.25	CT-S	90	C	240	200	0.015	—	280.2
2S-13	R	360	—	400	200	360	0.1	1.8	20	0.05	2.05	0.25	ST-S	90	C	240	200	0.015	—	141.4
2S-14	R	360	—	400	120	360	0.1	1.8	50	0.05	2.05	0.25	ST-S	90	C	240	200	0.015	—	190.4
2S-15	R	360	—	400	400	360	0.2	1.8	30	0.2	2.05	0.25	CT-S	90	C	240	200	0.015	—	182.1
2S-16	R	360	—	400	200	360	0.2	1.8	30	0.2	2.05	0.25	CT-S	90	C	240	200	0.015	—	197.8
2S-17	R	280	—	300	200	280	0.1	1.8	30	0.1	2.05	0.25	CT-S	90	C	240	200	0.015	—	143.2
2S-18	R	360	—	400	200	360	0.1	1.8	30	0.1	2.05	0.25	CT-S	90	C	240	200	0.015	—	172.9
2S-19	R	560	—	600	200	560	0.1	1.8	30	0.1	2.05	0.25	CT-S	90	C	240	200	0.015	—	247.9
U-jac.-1	R	360	—	400	200	360	0.1	1.8	30	0.05	2.05	0.25	ST-U	90	C	240	200	0.015	—	206.5
U-jac.-2	R	360	—	400	200	360	0.2	1.8	30	0.1	2.05	0.25	ST-U	90	C	240	200	0.015	—	229.1
U-jac.-3	R	360	—	400	200	360	0.3	1.8	30	0.15	2.05	0.25	ST-U	90	C	240	200	0.015	—	247.0
U-jac.-4	R	360	—	400	200	360	0.2	1.8	30	0.066667	2.05	0.25	ST-U	90	C	240	200	0.015	—	211.7

Table 1: Continued.

Specimen	Section	d_{fv}	h_f	h_w	b_w	d	nt_f	a/d	f'_c	ρ_{FRP}(%)	ρ_w(%)	ρ_s(%)	Configuration	β(degree)	Fiber	E_s	E_{FRP}	ε_{fu}	$V_{t(\exp)}$	$V_{t(NUM)}$
U-jac.-5	R	360	—	400	200	360	0.2	1.8	30	0.05	2.05	0.25	ST-U	90	C	240	200	0.015	—	205.9
U-jac.-6	R	360	—	400	200	360	0.2	1.8	30	0.2	2.05	0.25	CT-U	90	C	240	200	0.015	—	268.8
U-jac.-7	R	360	—	400	200	360	0.2	1.8	30	0.1	2.05	0.25	ST-U	90	C	240	200	0.015	—	201.9
U-jac.-8	R	360	—	400	200	360	0.2	1.8	30	0.1	2.05	0.25	ST-U	90	C	240	200	0.015	—	231.8
U-jac.-9	R	360	—	400	200	360	0.2	1.5	30	0.1	2.05	0.25	ST-U	90	C	240	200	0.015	—	242.7
U-jac.-10	R	360	—	400	200	360	0.2	2.25	30	0.1	2.05	0.25	ST-U	90	C	240	200	0.015	—	225.0
U-jac.-11	R	360	—	400	200	360	0.2	1.8	30	0.333333	2.05	0.25	CT-U	90	C	240	200	0.015	—	209.1
U-jac.-12	R	360	—	400	200	360	0.2	1.8	30	0.1	2.05	0.25	CT-U	90	C	240	200	0.015	—	360.2
U-jac.-13	R	360	—	400	200	360	0.1	1.8	20	0.05	2.05	0.25	ST-U	90	C	240	200	0.015	—	172.1
U-jac.-14	R	360	—	400	120	360	0.1	1.8	50	0.05	2.05	0.25	ST-U	90	C	240	200	0.015	—	243.9
U-jac.-15	R	360	—	400	400	360	0.2	1.8	30	0.2	2.05	0.25	CT-U	90	C	240	200	0.015	—	211.9
U-jac.-16	R	360	—	400	200	360	0.2	1.8	30	0.2	2.05	0.25	CT-U	90	C	240	200	0.015	—	246.7
U-jac.-17	R	280	—	300	200	280	0.1	1.8	30	0.1	2.05	0.25	CT-U	90	C	240	200	0.015	—	185.2
U-jac.-18	R	360	—	400	200	360	0.1	1.8	30	0.1	2.05	0.25	CT-U	90	C	240	200	0.015	—	210.5
U-jac.-19	R	560	—	600	200	560	0.1	1.8	30	0.1	2.05	0.25	CT-U	90	C	240	200	0.015	—	278.7
Wrapped-1	R	360	—	400	200	360	0.1	1.8	30	0.05	2.05	0.25	ST-W	90	C	240	200	0.015	—	255.4
Wrapped-2	R	360	—	400	200	360	0.2	1.8	30	0.1	2.05	0.25	ST-W	90	C	240	200	0.015	—	301.8
Wrapped-3	R	360	—	400	200	360	0.3	1.8	30	0.15	2.05	0.25	ST-W	90	C	240	200	0.015	—	322.8
Wrapped-4	R	360	—	400	200	360	0.2	1.8	30	0.066667	2.05	0.25	ST-W	90	C	240	200	0.015	—	272.2
Wrapped-5	R	360	—	400	200	360	0.2	1.8	30	0.05	2.05	0.25	ST-W	90	C	240	200	0.015	—	252.8
Wrapped-6	R	360	—	400	200	360	0.2	1.8	30	0.2	2.05	0.25	CT-W	90	C	240	200	0.015	—	355.8
Wrapped-7	R	360	—	400	200	360	0.2	1.8	30	0.1	2.05	0.25	ST-W	90	C	240	200	0.015	—	270.5
Wrapped-8	R	360	—	400	200	360	0.2	1.8	30	0.1	2.05	0.25	ST-W	90	C	240	200	0.015	—	305.7
Wrapped-9	R	360	—	400	200	360	0.2	1.5	30	0.1	2.05	0.25	ST-W	90	C	240	200	0.015	—	307.6
Wrapped-10	R	360	—	400	200	360	0.2	2.25	30	0.1	2.05	0.25	ST-W	90	C	240	200	0.015	—	272.1
Wrapped-11	R	360	—	400	200	360	0.2	1.8	30	0.333333	2.05	0.25	CT-W	90	C	240	200	0.015	—	288.3
Wrapped-12	R	360	—	400	200	360	0.2	1.8	30	0.1	2.05	0.25	CT-W	90	C	240	200	0.015	—	482.0
Wrapped-13	R	360	—	400	200	360	0.1	1.8	20	0.05	2.05	0.25	ST-W	90	C	240	200	0.015	—	209.1
Wrapped-14	R	360	—	400	120	360	0.1	1.8	50	0.05	2.05	0.25	ST-W	90	C	240	200	0.015	—	313.1
Wrapped-15	R	280	—	300	400	280	0.1	1.8	30	0.1	2.05	0.25	CT-W	90	C	240	200	0.015	—	217.8
Wrapped-16	R	360	—	400	200	360	0.1	1.8	30	0.1	2.05	0.25	CT-W	90	C	240	200	0.015	—	282.8
Wrapped-17	R	560	—	600	200	560	0.1	1.8	30	0.1	2.05	0.25	CT-W	90	C	240	200	0.015	—	435.0
Manos et al. [49]																				
CRB	R	322	—	360	200	322	—	2.79	22.4	—	2.43	—	—	—	—	202.7	—	—	39.44	39.44
CRBs	R	322	—	360	200	322	—	2.79	25.9	—	2.43	0.33	—	—	—	202.7	—	—	90.60825	87.89
RB200C	R	322	—	360	120	322	0.13	2.79	22.4	0.109167	2.43	—	ST-U	90	C	202.7	41.784	0.009	97.99	97.99
RB200Ca	R	322	—	360	120	322	0.13	2.79	22.4	0.109167	2.43	—	ST-U + anchorage	90	C	202.7	41.784	0.009	115.3301	118.79
RB200S	R	322	—	360	120	322	0.11	2.79	25.9	0.098667	2.43	—	ST-U	90	SFRP	202.7	36.35	0.009	94.12903	87.54
RB200Sa	R	322	—	360	120	322	0.11	2.79	25.9	0.098667	2.43	—	ST-U + anchorage	90	SFRP	202.7	36.35	0.009	122.25	112.47
RB150C	R	322	—	360	120	322	0.13	2.79	22.4	0.145556	2.43	—	ST-U	90	C	202.7	41.784	0.009	100.6566	99.65
RB150Ca	R	322	—	360	120	322	0.13	2.79	22.4	0.145556	2.439125	—	ST-U + anchorage	90	C	202.7	41.784	0.009	123.0408	120.58
RB150S	R	322	—	360	120	322	0.11	2.79	22.4	0.131556	2.439125	—	ST-U	90	SFRP	202.7	36.35	0.009	103.1383	96.95

Table 1: Continued.

Specimen	Section	d_{fv}	h_f	h_w	b_w	d	nt_f	a/d	f'_c	ρ_{FRP}(%)	ρ_w(%)	ρ_s(%)	Configuration	β(degree)	Fiber	E_s	E_{FRP}	ε_{fu}	$V_{t(\exp)}$	$V_{t(NUM)}$
RB150Sa	R	322	—	360	120	322	0.11	2.79	22.43	0.131556	2.439125	—	ST-U + anchorage	90	SFRP	202.7	36.35	0.009	118.7692	123.52
Qapo et al. [50]																				
Control	I	457.2	—	—	102	457.2	—	2.5	—	—	1.23	0	—	90	—	186.6-204.5	—	—	117.4	129,5
IB-05	I	457.2	—	—	102	457.2	1.25	2.5	70.8	1.466728	1.23	0	ST-U	90	C	186.6-204.6	6.585	0.015	161.9	162
IB-10	I	457.2	—	—	102	457.2	1.25	2.5	70.8	0.733364	1.23	0	ST-U	90	C	186.6-204.7	6.585	0.015	119.2	149.7
Ibars et al. [51]																				
U90S5-a	R	250	—	420	250	370	0.29	3.5	36.9	0.88	2.03	0.10	ST-U	90	C	200	240	0.015	341	341
U90S5-b	R	250	—	420	250	370	0.29	3.5	28.0	0.88	2.03	0.10	ST-U	90	C	200	240	0.015	326	315
U90S3-a	R	250	—	420	250	370	0.17	3.5	20.5	0.53	2.03	0.10	ST-U	90	C	200	240	0.0155	285	263
U90S3-b	R	250	—	420	250	370	0.17	3.5	22.5	0.53	2.03	0.10	ST-U	90	C	200	240	0.0155	204	—
U90S3-c	R	250	—	420	250	370	0.17	3.5	28.0	0.53	2.03	0.10	ST-U	90	C	200	240	0.0155	320	311
W90S5	R	370	—	420	250	370	0.29	3.5	49.9	0.88	2.03	0.10	ST-W	90	C	200	240	0.015	383	402
W90S3-ab	R	370	—	420	250	370	0.17	3.5	37	0.53	2.03	0.10	ST-W	90	C	200	240	0.0155	432	408
W90S3-b	R	370	—	420	250	370	0.17	3.5	37	0.53	2.03	0.10	ST-W	90	C	200	240	0.0155	394	408
Al Jawahery et al. [52]																				
Rf1 ∗ U90	R	—	—	—	150	260	0.3	2.4	44.5	0.177778	1.546154	—	ST-U	90	C	200	240	0.0204	233.24	225
A1 – 5INJ ∗	R	—	—	—	150	210-260	—	2.97-2.4	60	—	1.94-1.54	—	—	—	—	200	240	0.0204	113.5	118.2
A1-10U90	R	—	—	—	150	160-260	0.3	3.9-2.4	49	0.1	2.51-1.54	—	ST-U	90	C	200	240	0.0204	173.21	170.5
A2-10U45	R	—	—	—	150	160-260	0.3	3.9-2.4	51.5	0.1	2.51-1.55	—	ST-U	45	C	200	240	0.0204	171.523	160
A1 – 15U90 ∗	R	—	—	—	150	110-160	0.3	5.68-3.9	42.5	0.1	3.65-2.51	—	ST-U	90	C	200	240	0.0204	171.445	158
A2-15U45	R	—			150	110-260	0.3	5.68-2.4	60	0.1	3.65-1.54	—	ST-U	45	C	200	240	0.0204	168.149	164
Rf2U90	R	—	—	—	150	210	0.3	2.97	60.7	0.1	1.91	—	ST-U	90	C	200	240	0.0204	163.157	134
B1-5INJ	R	—	—	—	150	210-260	—	2.97-2.4	58.5		1.91-1.54	—	—	—	—	200	240	0.0204	108	152.8
B1-10U90	R	—	—	—	150	210-310	0.3	2.97-2.01	44	0.1	1.91-1.29	—	ST-U	90	C	200	240	0.0204	140.049	130.8
B2-10U45	R	—	—	—	150	210-310	0.3	2.97-2.02	61	0.1	1.91-1.30	—	ST-U	45	C	209 (assumed)	240	0.0204	153.45	110
B1-15U90	R	—	—	—	150	210-360	0.3	2.97-1.73	62	0.1	1.91-1.11	—	ST-U	90	C	200	240	0.0204	140.74	136
B2-15U45	R	—	—	—	150	210-360	0.3	2.97-1.73	50.1	0.1	1.91-1.11	—	ST-U	45	C	200	240	0.0204	119.664	110
Jin et al. [53]																				
CBF-S-0.0555	R	180	—	200	80	180	1	2	39.5	0.0555	1.24	0.12	ST-S	90	C	210	212	0.0198	—	—
CBF-M-0.0555	R	360	—	400	160	360	2	2	39.5	0.0555	1.24	0.12	ST-S	90	C	210	212	0.0198	—	—
CBF-L-0.0555	R	540	—	600	240	540	3	2	39.5	0.0555	1.24	0.12	ST-S	90	C	210	212	0.0198	—	—
CBF-U-0.0555	R	720	—	800	320	720	4	2	39.5	0.0555	1.24	0.12	ST-S	90	C	210	212	0.0198	—	—
CBF-S-0.111	R	180	—	200	80	180	2	2	39.5	0.111	1.24	0.12	ST-S	90	C	210	212	0.0198	—	—
CBF-M-0.111	R	360	—	400	160	360	4	2	39.5	0.111	1.24	0.12	ST-S	90	C	210	212	0.0198	—	—

Table 1: Continued.

Specimen	Section	d_{fv}	h_f	h_w	b_w	d	nt_f	a/d	f'_c	ρ_{FRP}(%)	ρ_w(%)	ρ_s(%)	Configuration	β(degree)	Fiber	E_s	E_{FRP}	ε_{fu}	$V_{t(\text{exp})}$	$V_{t(\text{NUM})}$
CBF-L-0.111	R	540	—	600	240	540	6	2	39.5	0.111	1.24	0.12	ST-S	90	C	210	212	0.0198	—	—
CBF-U-0.111	R	720	—	800	320	720	8	2	39.5	0.111	1.24	0.12	ST-S	90	C	210	212	0.0198	—	—
CBF-S-0.222	R	180	—	200	80	180	4	2	39.5	0.222	1.24	0.12	ST-S	90	C	210	212	0.0198	—	—
CBF-M-0.222	R	360	—	400	160	360	8	2	39.5	0.222	1.24	0.12	ST-S	90	C	210	212	0.0198	—	—
CBF-L-0.222	R	540	—	600	240	540	12	2	39.5	0.222	1.24	0.12	ST-S	90	C	210	212	0.0198	—	—
CBF-U-0.222	R	720	—	800	320	720	16	2	39.5	0.222	1.24	0.12	ST-S	90	C	210	212	0.0198	—	—
CBF-S-1.11	R	180	—	200	80	180	20	2	39.5	1.11	1.24	0.12	ST-S	90	C	210	212	0.0198	—	—
CBF-M-1.11	R	360	—	400	160	360	40	2	39.5	1.11	1.24	0.12	ST-S	90	C	210	212	0.0198	—	—
CBF-L-1.11	R	540	—	600	240	540	60	2	39.5	1.11	1.24	0.12	ST-S	90	C	210	212	0.0198	—	—
CBF-U-1.11	R	720	—	800	320	720	80	2	39.5	1.11	1.24	0.12	ST-S	90	C	210	212	0.0198	—	—
CBF-S-2.22	R	180	—	200	80	180	40	2	39.5	2.22	1.24	0.12	ST-S	90	C	210	212	0.0198	—	—
CBF-M-2.22	R	360	—	400	160	360	80	2	39.5	2.22	1.24	0.12	ST-S	90	C	210	212	0.0198	—	—
CBF-L-2.22	R	540	—	600	240	540	120	2	39.5	2.22	1.24	0.12	ST-S	90	C	210	212	0.0198	—	—
CBF-U-2.22	R	720	—	800	320	720	160	2	39.5	2.22	1.24	0.12	ST-S	90	C	210	212	0.0198	—	—
CBF-S-4.44	R	180	—	200	80	180	80	2	39.5	4.44	1.24	0.12	ST-S	90	C	210	212	0.0198	—	—
CBF-M-4.44	R	360	—	400	160	360	160	2	39.5	4.44	1.24	0.12	ST-S	90	C	210	212	0.0198	—	—
CBF-L-4.44	R	540	—	600	240	540	240	2	39.5	4.44	1.24	0.12	ST-S	90	C	210	212	0.0198	—	—
CBF-U-4.44	R	720	—	800	320	720	320	2	39.5	4.44	1.24	0.12	ST-S	90	C	210	212	0.0198	—	—
CBF-S-8.88	R	180	—	200	80	180	160	2	39.5	8.88	1.24	0.12	ST-S	90	C	210	212	0.0198	—	—
CBF-M-8.88	R	360	—	400	160	360	320	2	39.5	8.88	1.24	0.12	ST-S	90	C	210	212	0.0198	—	—
CBF-L-8.88	R	540	—	600	240	540	480	2	39.5	8.88	1.24	0.12	ST-S	90	C	210	212	0.0198	—	—
CBF-U-8.88	R	720	—	800	320	720	640	2	39.5	8.88	1.24	0.12	ST-S	90	C	210	212	0.0198	—	—

Table 2: Database of numerical studies assessing parameters of RC beams strengthened in shear with FRP bars and validating with experimental tests.

Database of FE conducts on reinforce concrete beam strengthened by FRP bars											
Geometry of beams					Properties of concrete			Configuration		Results	
Specimen	Section	d (mm)	Bw (mm)	a/d	f_c'	ρ_w(%)	ρ_s(%)	Fiber	Configuration	$V_{t(\exp)}$ (KN)	$V_{t(\mathrm{NUM})}$ (KN)
Hawileh et al. [54]											
FE SPEC-1	R	320	200	5	25	1.79	0	G	NSM	92.68	95.05
Godat et al. [55]											
S0-ETS	T	350	152	3	25	0.35	0	C	ETS	273	301.4
S1-ETS	T	350	152	3	25	0.35	0.3779	C	ETS	397	417.9
S3-ETS	T	350	152	3	25	0.35	0.2543	C	ETS	425.5	428
Qapo et al. [56]											
S0-12d130s	T	350	152	3	25	0.35	0	C	ETS	180.8	179.6
1-12d260s	T	350	152	3	25	0.35	0.3779	C	ETS	266.6	271.5
R00	T	295	125	3.05	17.4	1.77	0.292	C	ETS	142	150.6
Specimen 8	R	189	110	3.17	47	0.934	0	A	ETS	32	33.3
Specimen 9	R	189	110	3.17	47	0.934	0	A	ETS	32	31.9
Specimen 10	R	189	110	3.17	47	0.394	0	A	ETS	30	31.5
Hawileh et al. [57]											
B1	R	200	300	3.5/11.5	52.3	0.28	0	C	FRP bars	84	81.1
B2	R	300	300	3.5/6.5	52.3	0.35	0	C	FRP bars	94	81.6
B3	R	400	300	3.5/4	52.3	0.58	0	C	FRP bars	102	91.9
B4	R	500	300	3.5/2.5	52.3	0.58	0	C	FRP bars	162	161.6
B5	R	400	300	6.5/1	52.3	0.58	0	C	FRP bars	381	417.5
B6	R	400	300	6/1.5	52.3	0.73	0	C	FRP bars	309	313.2
Shomali et al. [58]											
B3-NSM-30	R	262	200	2.29	32	1.79	0	C	NSM	210	224.7
B4-NSM-30	R	262	200	2.29	34	1.79	0.264	C	NSM	262	280.34

the crack shape and varies with the amount of internal steel reinforcement. Therefore, the authors present the following equation to cover all shear crack shapes:

$$w = w_{\max} \begin{cases} \dfrac{1 - C_{\bar{z}}}{1 - C} \times \bar{z} & 0 \le C < \dfrac{1}{2}, \\ 4C_{\bar{z}}(1 - C_{\bar{z}}) & \dfrac{1}{2} \le C < 1, \end{cases} \tag{2}$$

where w = crack width, $w_{\max}$ = maximum crack width [9], $\bar{z} = z/z_b$ (normalized vertical coordinate where $z_b = 0.9\,d$, the effective depth of the beam), and C is the factor determining the shape of the strain distribution. Among the 239 studied beams, 102 beams (42.6%) were evaluated for their crack width, crack pattern, and shape function (Figure 4). However, only two studies [6, 7], involving 10 beams (4.1%), considered the effect of crack shape and crack function in their proposed shear model based on FEA. The rest (92 beams) focused on shear crack patterns. This indicates the need for more research related to shear crack shape functions, considering different crack shapes and their effect on the distribution factors and the effective stress and strain, to develop future predictive models.

4.2. Strain, Stress, and Slip Distribution along the Diagonal Crack on EB FRP. Chen and Teng [8] showed that the width of the shear crack varies along its length, confirming thereby that the strain and stress distributions along the FRP laminates/fabrics are nonuniform. As for the issue that FRP laminates/fabrics crossed by the diagonal shear crack experience different ranges of strain and stress as the crack widens, it could be concluded that the amount of stress/strain in the fibers is influenced by the crack width, and hence, the D_{FRP} distribution factor is not constant. Therefore, D_{FRP} depends on the location of the FRPs because the fibers located at the end of the crack experience more strain than those situated at the tip of the crack. Nevertheless, as mentioned in the previous section, the shape of the shear crack relies on the steel reinforcement, and hence, the shear crack is not necessarily linear. The maximum width of the crack can be in the middle of the beam if the beam contains a high ratio of longitudinal steel reinforcement [7]. The other factor affecting the fiber strain distribution is the FRP configuration type. For instance, when assuming U-shaped configurations, fibers located below the shear crack experience more strain than those located near the top of the crack because there is enough bond length on the lower side of crack compared to the upper side. However, for side-bonded configurations, with the same bond length at the bottom and top of the crack, the fibers on both sides of the crack experience the same strain distribution. Therefore, it is of paramount importance to consider the strain profile

Table 3: Database of numerical studies assessing distribution of stress and strain on the interface and interaction between steel stirrups and FRP composites of RC beams strengthened in shear with externally FRP composites.

FE conducts on behavior of interface and interaction between internal and external reinforcements								
Specimen	Section	Interaction between concrete and FRP	Configuration	FE program	Studied parameters along the diagonal shear crack			
Lu et al. [7]								
Crack model A, U-jacketing	R	Lu et al. [16]	CT-U	ANSYS	Slip distribution on the interface	Stress distribution on FRP	Stress distribution factor	Shear crack shape
Crack model B, U-jacketing	R	Lu et al. [16]	CT-U	ANSYS	Slip distribution on the interface	Stress distribution on FRP	Stress distribution factor	Shear crack shape
Crack model C, U-jacketing	R	Lu et al. [16]	CT-U	ANSYS	Slip distribution on the interface	Stress distribution on FRP	Stress distribution factor	Shear crack shape
Crack model D, U-jacketing	R	Lu et al. [16]	CT-U	ANSYS	Slip distribution on the interface	Stress distribution on FRP	Stress distribution factor	Shear crack shape
Crack model A, side-bonding	R	Lu et al. [16]	CT-S	ANSYS	Slip distribution on the interface	Stress distribution on FRP	Stress distribution factor	Shear crack shape
Crack model B, side-bonding	R	Lu et al. [16]	CT-S	ANSYS	Slip distribution on the interface	Stress distribution on FRP	Stress distribution factor	Shear crack shape
Crack model C, side-bonding	R	Lu et al. [16]	CT-S	ANSYS	Slip distribution on the interface	Stress distribution on FRP	Stress distribution factor	Shear crack shape
Crack model D, side-bonding	R	Lu et al. [16]	CT-S	ANSYS	Slip distribution on the interface	Stress distribution on FRP	Stress distribution factor	Shear crack shape
Chen et al. [6]								
Specimen	Section	Interaction between components: FRP vs. steel stirrups	Interaction between components: FRP vs. concrete	Configuration	FE program	Studied parameters along the diagonal shear crack		
FRP side strips	R	Code [5]	Lu et al. [16]	ST-S	ABAQUS	Mobilization factor for steel stirrups and FRP as crack widens	Stress distribution on FRP	
FRP U-strips	R	Code [5]	Lu et al. [16]	ST-U	ABAQUS	Mobilization factor for steel stirrups and FRP as crack widens	Stress distribution on FRP	

on the fibers to obtain the effective strain in FRP laminates/fabrics. On the other hand, studying slip profiles on the interface layer gives an insight into how the interface layer responds to increasing load and crack propagation. The slip distributions make it possible to understand how shear cracks form because fiber debonding occurs near the shear crack. Therefore, through a slip profile, shear crack propagation can be predicted by FEA, which is not possible by experimental tests. Among the 239 beams, 84 (35.1%) beams were subjected to FEA that evaluated the strain distribution along the fibers and the slip profile along the interface layer, of which 25 beams (10.4%) were T-shaped cross sections (Figure 4). This indicates the need for more FE studies on the strain and slip profile for T cross section beams.

4.3. Load-Deflection Curve. Most laboratory and FE results on RC beams strengthened in shear using FRP composites have been based on the load-deflection curve, particularly in experimental tests. Generally, the load-deflection response has become the way to evaluate the ultimate load-carrying capacity as well as the ductility and the behavioral features of EB-FRP shear-strengthened RC beams. In fact, the load-deflection response has become a criterion to validate the accuracy of FEA results against experimental results. However, it cannot be the only criterion for validating FEA and developing analytical models because it has been observed that, even if the load-deflection curves of shear-strengthened RC beams using EB-FRP were compatible when subjected to two different tests, their failure modes could be different. In addition, it has been established that specimens featuring the same load-deflection responses from different tests may present many discrepancies with regard to formation and number of shear cracks, strain

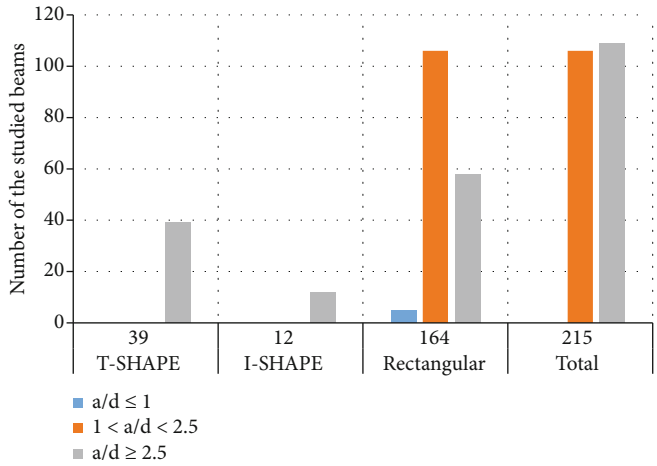

Figure 2: Number of cross section types and a/d ratios considered in FEA.

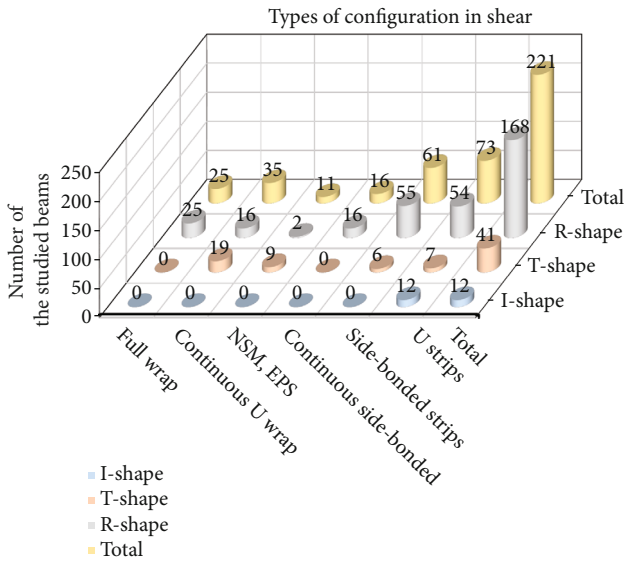

Figure 3: Number of cross section types and configurations considered in FEA.

profile along fibers, and slip profiles along the interface, as well as fiber strain distribution along the horizontal axis of the specimens. Nevertheless, the load-deflection response can be one of the indications to validate whether a simulated model is accurate. Among the 239 beams, 185 (77.4%) FE beams were studied in terms of load-deflection response, of which 125 (52.3%) were rectangular, 48 (20%) were T-shaped, and 12 (5%) were I-shaped cross sections (Figure 4).

4.4. Number, Size, and Types of Elements in Simulation. Selecting the right element in simulation for each component of the beam is of paramount importance in FE methods, which are highly sensitive to the size and type of the elements. As the size of elements is reduced, the time and cost for FEA will increase. Modeling EB-FRP RC beams can be classified into two categories: (i) three-dimensional simulation, which is time-consuming but provides results that are representative of the real model and (ii) two-dimensional modeling, which takes advantage of the plane stress behavior that EB-FRP RC beams can exhibit. The two-dimensional model ignores the deflection of the beam into the normal direction to its plane and makes some further simplifying assumptions, reducing considerably the time and cost of FEA. In the three-dimensional model, the brick element is chosen for concrete, whereas for steel reinforcement, either the one-dimensional bar or the three-dimensional brick element can be considered. For EB-FRP laminates/fabrics, the two-dimensional shell element for EB-FRP and the one-dimensional link or bar elements would be appropriate. As for concrete-to-FRP and steel reinforcement-to-concrete interface elements, there are many options affecting the right choice, depending on the type of fibers in the EB-FRP (one-directional, two-directional) and ranging from the one-dimensional link element to three-dimensional cohesive elements depending on whether the model in question is three- or two-dimensional. Few investigations considered the effect of element type as a studied parameter in FE simulations. In fact, only 17 (7.1%) of the 239 beams underwent this study, of which 12 (5%) were rectangular and 5 (2%) were T-shaped cross sections (Figure 4).

4.5. Effective Stress and Strain, Bond Length, and Distribution Factor (D). The effective stress and strain experienced by FRP are essential components to calculate FRP contribution to shear resistance, which depends on the stress and strain distribution along the shear cracks, which in turn relies on the shape functions of cracks. As for the effective bond length of EB-FRP, which is the length of FRP that has not debonded and hence still contributes to the shear resistance, it is directly related to the shear crack distribution in the concrete. Indeed, the more the shear cracks are distributed, the shorter is the effective bond length of the FRP, and the more likely the beam will exhibit a premature failure [10]. Many models based on the effective bond length have been reported in the literature. The models introduced by Neubauer and Rostasy [11] and Chen and Teng [12] are

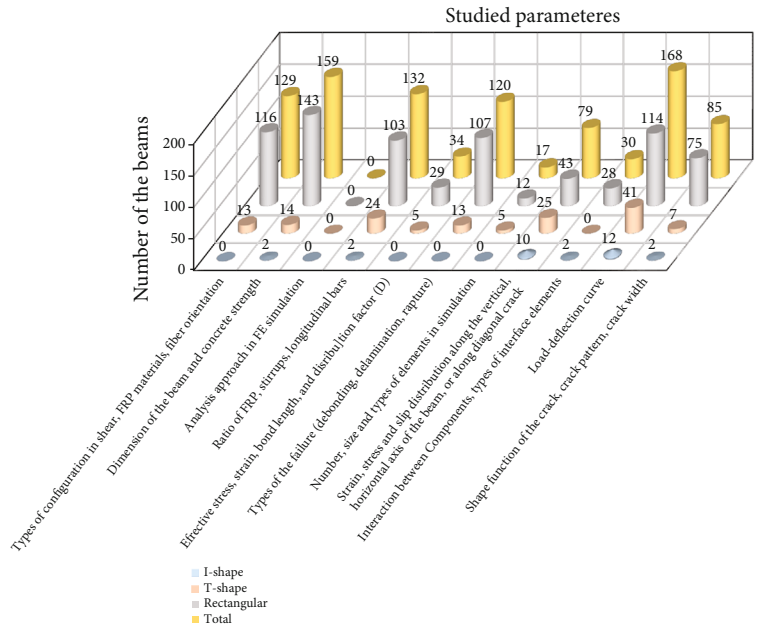

Figure 4: Number of studied beams evaluating the effect of each parameter on closed-form model for shear contribution of FRP composites by FEA.

some of the most reliable models, which are expressed in the following Equations (3)–(4), respectively:

$$L_e = \sqrt{\frac{E_f t_f}{2 f_{ct}}}, \tag{3}$$

where f_{ct} is the tensile strength of concrete [13]:

$$f_{ct} = 0.53\sqrt{f'_c}, \tag{4}$$

$$L_e = \sqrt{\frac{E_{\text{frp}} t_{\text{frp}}}{\sqrt{f'_c}}}. \tag{5}$$

Among the 239 RC beams strengthened in shear using FRP composites, only 41 (17.1%) were considered to study the effective stress and strain, the bond length, and distribution factor (D), of which 29 (12.1%) were rectangular and 12 (5%) were T-shaped cross sections (Figure 4).

4.6. Failure Modes in Concrete and EB-FRP (Debonding, Delamination, Rupture). Failure of RC beams strengthened in shear using EB-FRP can be mainly related either to reinforced concrete (crushing of concrete struts, tensile shear failure, yielding and fracture of steel reinforcement) or to EB-FRP composites (debonding or rupture). In fact, the failure modes observed in EB-FRP specimens are (i) rupture of FRP laminates/fabrics, which occurs usually in a fully wrapped FRP configuration; (ii) debonding of FRP due to lack of effective bond length near shear cracks; and (iii) failure of RC beams due to delamination of EB laminates/fabrics from the concrete substrate when EB-FRP still contributes to the shear resistance [9]. Failure modes related to loss of concrete strength also depend on the shear span-to-depth ratio, according to Teng et al. [14]. They can involve compressive or tensile shear failure of the RC beams, as well as failure of deep beams. The failure modes of 124 (51.8%) beams were subjected to FE studies, of which 113 (47.2%) were rectangular and only 11 (4.6%) were T-shaped cross sections (Figure 4). The advantage of FE studies over experimental tests is that detection of failure modes using FEA is much easier than laboratory testing of shear-strengthened RC beams using EB-FRP. In addition, the post-failure response of the specimens can be captured using FEA, which is impossible in an experimental protocol.

4.7. Shear Strengthening Configurations, FRP Materials, and Fiber Orientation. There is an array of configurations for strengthening RC beams in shear, which are associated with the beam's cross section, shear crack orientation, and accessibility to the surfaces of the beam to be strengthened. Three EB configurations are used in practice for strengthening RC beams in shear: (i) the side-bonded configuration where FRP laminates/fabrics are installed on the two lateral sides of the beam. The corresponding failure mode is mainly by FRP delamination from the concrete substrate; (ii) the U-shaped configuration where the FRP laminates/fabrics are installed on three surfaces of the beam (lateral sides and soffit of the beam). The corresponding failure mode is mainly by FRP debonding from the top side of the shear crack due to lesser effective bond length compared to the bottom side of crack, and (iii) the full-wrap configuration is usually labeled by the symbol W and involves wrapping FRP laminates/fabrics over the whole surface of the beam. The full-wrap configuration is more applicable to beams with easy access to all beam surfaces, such as rectangular RC beams and columns. All three configurations can be installed to

the concrete substrate in the form of continuous or discontinuous (strips) bonded FRP composites. If bond length is insufficient, anchorages can be used to prevent premature debonding failure. Furthermore, various types of fibers are used for FRP composites, such as carbon, glass, and aramid. The fiber orientation in FRP laminates/fabrics can be horizontal, vertical, or diagonal at any angle to the axis of RC beams. When feasible, the optimal fiber orientation would cross the shear crack perpendicularly, providing more contribution to shear resistance. 140 (58.5%) of the 239 beams were subjected to FEA to evaluate the effect of shear strengthening configurations, type of FRP composites, and fiber orientation, of which 127 (53.1%) were rectangular and only 13 (5.4%) were T-shaped cross sections (Figure 4).

4.8. Analytical Approach in FE Simulations. Solving problems using FEA can be classified into two techniques: (i) static solvers and (ii) dynamic solvers, which can further be divided into dynamic implicit and dynamic explicit. Because ABAQUS/CAE 2017 was used in the majority of studies, the following description is concentrated on ABAQUS solvers. A dynamic analysis is to be privileged over static analysis because of many reasons and considerations, such as the brittle behavior of concrete, debonding phenomenon, delamination of concrete substrate, problem of reaching convergence in analysis, and the postpeak behavior of RC beams strengthened in shear using EB-FRP laminates/sheets. Nevertheless, results obtained from a dynamic approach should be verified against a general static analysis. When performing dynamic analysis on specimens, certain parameters should be considered to improve the accuracy of the results. These include the loading pattern (smoothing, stepping, or ramping), loading duration on the structure, amount of damping for EB-FRP RC beams, and time increment, among others [9]. Figure 4 reveals that among all the FEA studies, none of them mentioned how these influencing parameters were selected to solve their models. Therefore, when the dynamic solver is used, an explanation should be provided of how these parameters were selected in the implicit or the explicit analysis.

4.9. Interaction between Components and Types of Interface Elements. Steel stirrups and EB-FRP composites are the two main factors that contribute to shear resistance in EB-FRP strengthened RC beams. Nevertheless, Bousselham and Chaallal [15] showed an inverse interaction between EB-FRP and steel stirrups. The contribution of EB-FRP to shear resistance was found to decrease as the ratio of rigidity of steel stirrups to EB-FRP $(E_s\rho_s/E_f\rho_f)$ increased, confirming thereby the interaction between internal and external reinforcement. Chen et al. [6] introduced a model that explained this inverse shear interaction between steel stirrups and EB-FRP and demonstrated that because of this inverse interaction, neither internal nor external reinforcement reaches its full capacity. Therefore, two mobilization factors were proposed by Chen et al. [6] for determining the contribution of steel stirrups and FRP in EB-FRP RC beams:

$$V_u = V_c + K_s V_s + K_f V_f, \tag{6}$$

where K_f and K_s are the mobilization factors accounting for FRP and steel stirrups and varying between 0 and 1. Chen et al. [6] investigated the response of these two mobilization factors and found that K_f and K_s could be functions of crack width. The authors then created artificial cracks and observed the response of the two mobilization factors as the cracks grew, using two configuration types (U-shaped and side-bonded). They showed that as the crack width increases, K_f was always greater than K_s, which means that when most of the FRP strips were already debonded or had reached their maximum strength, the steel stirrups had not yet reached their maximum strength.

They further showed that there was an opposite behavior between K_f and K_s, indicating an inverse interaction, in which K_s was always less than K_f, and that this inverse interaction reduced the FRP shear contribution more than when the effect of this interaction was not considered. Hence, if the effect of this inverse interaction on just the contribution of FRP strips is considered, based on the equation proposed by Chen et al. [6], the following equation can be derived, in which the effect of inverse interaction is considered by means of a coefficient K:

$$V_u = V_c + V_s + KV_f. \tag{7}$$

Integrating Equation (6) and Equation (7), it follows that [9]:

$$K = K_f + (K_s - 1) \times \frac{V_s}{V_f} = K_f + (K_s - 1) \times \mu, \tag{8}$$

where:

$$\mu = \frac{V_s}{V_f} = \frac{f_y A_{\text{sv}}}{f_{f,e} A_{\text{frp}}}. \tag{9}$$

This indicates that when the amount of steel stirrups, and consequently the value of μ increases, the value of K_f declines [9, 15]. From the database, approximately 100 EB-FRP RC beams were considered in this study to evaluate the response of inverse shear interaction between steel stirrups and EB-FRP, with different EB-FRP configurations (continuous U-shaped, strip U-shaped, fully wrapped, and side-bonded) and based on steel stirrups ratio, EB-FRP ratio, and gain in shear contribution, as shown in Figures 5(a)–5(d). The figures show that the shear gain due to FRP decreased by increasing the ratio of steel stirrups, which confirms the research findings by Bousselham and Chaallal [15]. In addition to the ratio of steel stirrups and EB-FRP, other factors, like the FRP configuration or the size effect, could have affected this inverse shear interaction because this database

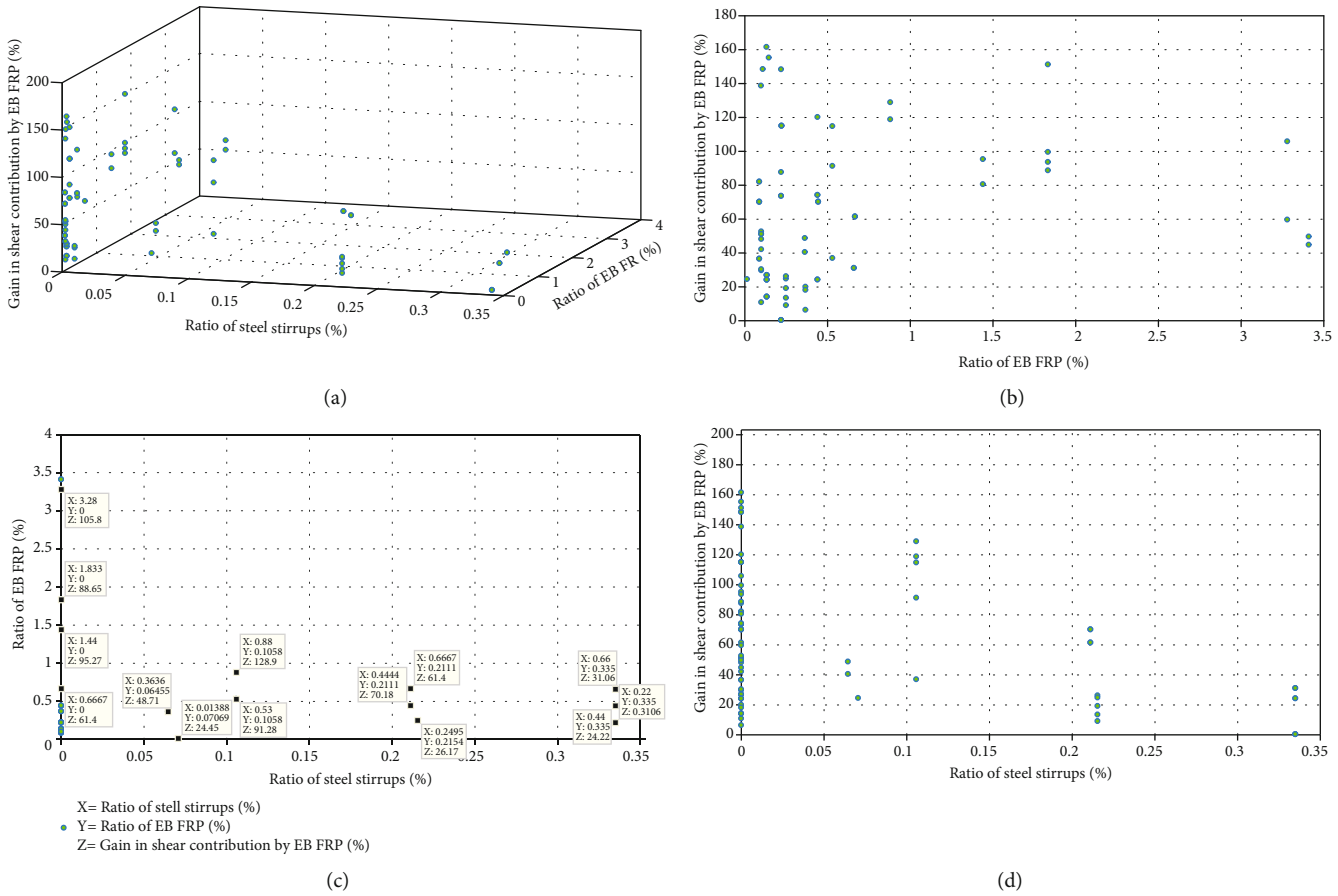

Figure 5: Interaction between steel stirrups and EB-FRP versus shear gain contributions.

considers all types of shear configurations and beam sizes. The FRP gain contribution can be computed as follows:

$$\text{FRP gain contribution} = \frac{V_f}{\left(V_t - V_f\right)}, \tag{10}$$

where V_t is the total shear resistance of the beam and V_f is the contribution of FRP to shear resistance.

Among the 239 beams, only 44 (20%) beams were subjected to FEA that considered the interaction between all components simultaneously (concrete, steel reinforcement, and FRP composites), based on the modeling of concrete cracking, of which 12 (5%) beams assumed a properly defined bond-slip law using a smeared crack + crack band model for both concrete-to-FRP and concrete-to-steel interactions, as illustrated in Figure 6. Moreover, for only 16 (6.7%) and 10 (4.1%) of the beams, a bond-slip law with smeared crack + crack band model was assumed for concrete-to-FRP and for concrete-to-steel interactions, respectively. Therefore, if the inverse interaction with concrete is considered as a fact in the overall response of RC beams strengthened in shear using FRP composites, both interactions for internal and external reinforcement should be introduced to the FE package alongside the smeared crack + crack band model. Accordingly, the simulated model would be representative of the real beam, and the results obtained from the FE package would be more reliable. In the current study, as the database shows, only 5% of all specimens were adequately and correctly modeled and simulated. Therefore, there is a need for more studies with precise and accurate simulations of RC beams strengthened in shear using FRP and particularly the EB strengthening technique. The aim of these studies would be to measure the effective strains and stresses using precise FE simulations to incorporate their effects into a reliable closed-form model providing the contribution of FRP composites to shear resistance of FRP-strengthened RC beams.

4.10. Interface Elements between Concrete and FRP Composites. There are few models in the FE software that can be introduced as an interface element between concrete and FRP, ranging from one-dimensional elements (e.g., link, spring, and truss) to 2-dimensional or 3-dimentsional elements. They stand for the behavior of the interface layer (interfacial shear stress, slip profile along the interface layer). As for the 2-dimensional interface elements, cohesive elements existing in all FE software's could be an appropriate candidate to simulate the response of the interface layer in its plane. Indeed, precision of results obtained from the

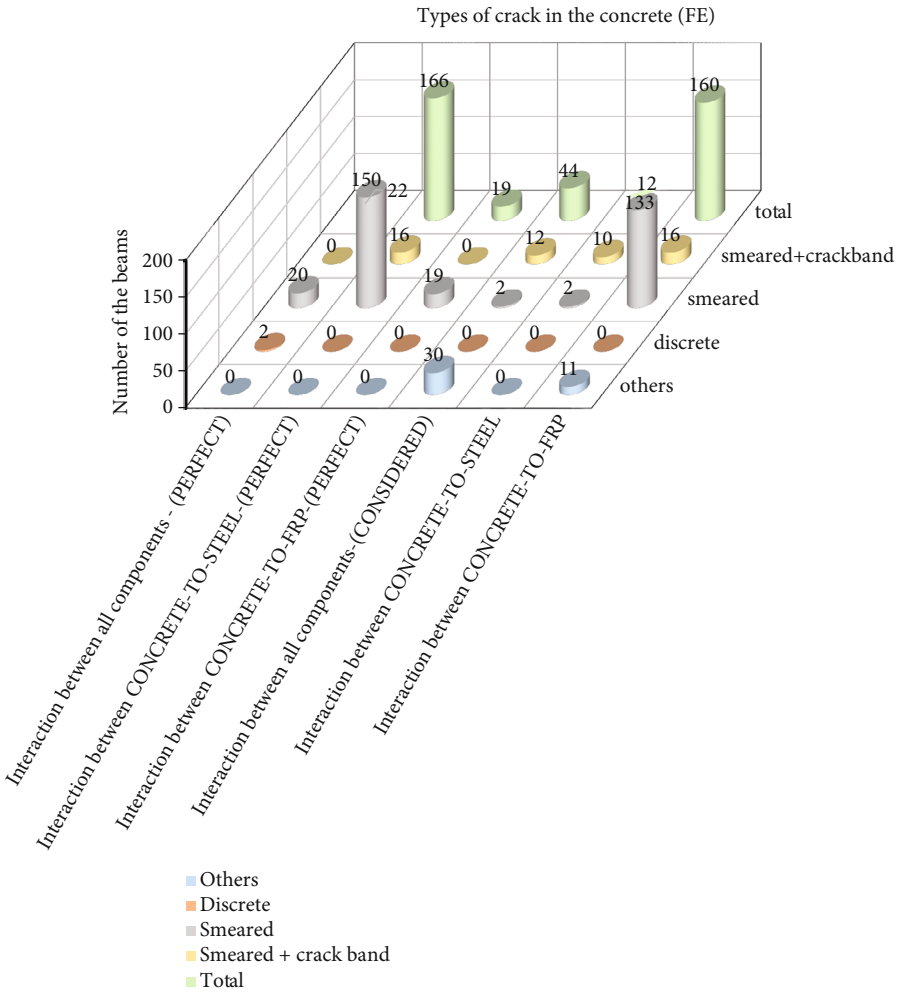

Figure 6: Number of studied beams evaluating bond-models based on definition of types of crack for concrete by FEA.

behavior of interface layer much depends on the model introduced to those elements, which can be obtained from both numerical and experimental tests. Few studies have been conducted on the response of bond-slip models, which are described hereafter. Since the failure modes at the interface layer could be different (debonding, delamination), the one-dimensional elements are not an appropriate representative for presenting the response of the debonding failure at the interface layer. However, most of the research studies carried out on the 2-dimensional interface elements (cohesive elements) concentrated on the behavior of the interface layer in its plane (failure modes 2 and 3), ignoring the delamination failure occurring normal to the cohesive plane (delamination phenomenon, failure mode 1). Therefore, it is of paramount importance that 2-dimensional or 3-dimensional elements should be implemented as an interface layer to consider all types of failure modes (1, 2, and 3), by representing the debonding in 2-directions of the interface elements at its plane and the delamination normal to the interface elements. According to the study conducted by Lu et al. [16], the following are the most reliable models accounting for the response of bond-slip models.

The relationship proposed by Neubauer and Rostasy [11] for the bond-slip model consisted of two parts:

$$\tau = \tau_{\max}\left(\frac{s}{s_0}\right) \text{ If } s \le s_0 \text{for the ascending part of the curve,} \tag{11}$$

0 If $s > s_0$ for the descending part of curve,
where

$$\begin{aligned} \tau_{\max} &= 1.8\beta_w f_t, \\ s_0 &= 0.202\beta_w, \\ \beta_w &= \sqrt{1.125\left(\frac{\left((2-b_f)/b_c\right)}{\left((1+b_f)/400\right)}\right)}. \end{aligned} \tag{12}$$

Nakaba et al. [17] proposed the following relationship in which both ascending and descending parts are shown as an integrated curve:

$$\tau = \tau_{\max}\left(\frac{s}{s_0}\right)\left[\frac{3}{(2+(s/s_0)^3}\right] \text{For both ascending and descending part,} \tag{13}$$

where

$$\begin{aligned} \tau_{\max} &= 3.5{f'}^{0.19}, \\ s_0 &= 0.65. \end{aligned} \tag{14}$$

Monti et al. [18] applied two different equations for the ascending and descending part of the bond-slip curve:

$$\begin{aligned} \tau &= \tau_{\max}\left(\frac{s}{s_0}\right) \text{If } s \le s_0, \\ \tau &= \frac{s_f - s}{s_f - s_0} \text{ If } s > s_0, \end{aligned} \tag{15}$$

where

$$\begin{aligned} \tau_{\max} &= 1.8\beta_w f_t, \\ s_0 &= 2.5\tau_{\max}\left(\frac{t_a}{E_a} + \frac{50}{E_c}\right), \\ s_f &= 0.33\beta_w, \\ \beta_w &= \sqrt{\frac{1.5\left((2-b_f)/b_c\right)}{\left((1+b_f)/100\right)}}. \end{aligned} \tag{16}$$

Savoia et al. [19] employed just a united curve for both ascending and descending parts:

$$\tau_{\max} = \left(\frac{s}{s_0}\right)\left[\frac{2.86}{(1.86+(s/s_0))^{2.86}}\right] \text{For both ascending and descending part} \tag{17}$$

Where $\tau_{\max} = 3.5{f_c'}^{0.19}$, and $s_0 = 0.051$

Dai and Ueda [20] proposed to separate the equations for the ascending and descending sections of the curve:

$$\begin{aligned} \tau &= \tau_{\max}\left(\frac{s}{s_0}\right)^{0.575} \text{If } s \le s_0, \\ \tau &= \tau_{\max} e^{-\beta(s-s_0)} \text{If } s > s_0, \end{aligned} \tag{18}$$

where

$$\begin{aligned} \tau_{\max} &= \frac{-1.575\alpha K_a + \sqrt{2.481\alpha^2 {K_a}^2 + 6.3\alpha\beta^2 K_a G_f}}{2\beta}, \\ s_0 &= \frac{\tau_{\max}}{\alpha K_a}, \\ \beta &= 0.0035 K_a \left(\frac{E_f T_f}{1000}\right)^{0.34}, \\ G_f &= 7.554 {K_a}^{-0.449}\left(f_c'\right)^{0.343}, \\ K_a &= \frac{G_a}{t_a}. \end{aligned} \tag{19}$$

Another model proposed by Ueda et al. [21] in which the integrated equation is proposed for both ascending and descending parts of the curve:

$$\tau = 2UG_f\left(e^{-Us} - e^{-2Us}\right), \tag{20}$$

where

$$\begin{aligned} lpcU &= 6.846\left(\frac{E_f t_f}{1000}\right)^{0.108}\left(\frac{G_a/t_a}{1000}\right)^{0.833}, \\ G_f &= 0.446\left(\frac{E_f t_f}{1000}\right)^{0.023}\left(\frac{G_a/t_a}{1000}\right)^{-0.352} f_c'^{0.236}. \end{aligned} \tag{21}$$

Finally, the bond-slip model introduced by [16], which is the most accepted model used worldwide by researchers, is as follows:

For ascending and softening parts of bond-slip curve, the following models are applied:

$$\begin{aligned} \tau &= \tau_{\max}\sqrt{\frac{s}{s_0}} \text{If } s \le s_0, \\ \tau &= \tau_{\max} e^{-\alpha((s/s_0)-1)} \text{ If } s > s_0, \end{aligned} \tag{22}$$

where

$$\begin{aligned} s_0 &= 0.0195\beta_w f_t, \\ G_f &= 0.308{\beta_w}^2\sqrt{f_t}, \\ \alpha &= \frac{1}{\left(G_f/\tau_{\max}s_0\right) - (2/3)}, \\ \beta_w &= \sqrt{\frac{2-\left(w_f/\left(s_f \sin\beta\right)\right)}{1+\left(w_f/\left(s_f \sin\beta\right)\right)}}, \\ \beta &= \text{Orientation of the fiber.} \end{aligned} \tag{23}$$

In direction normal to the cohesive layer, which is representative of delamination in the interface, the following is for

estimation of initial stiffness of cohesive layer:

$$K_{nn} = \frac{1}{(t_{concrete}/E_{concrete}) + (t_{epoxy}/E_{epoxy})}. \quad (24)$$

4.11. Interface Elements between Concrete and Steel Reinforcement. Unlike the interface layer between concrete and FRP where all 3 modes of failure should be defined (from one-dimensional to 2- and 3-dimensional elements), the interface between concrete and steel bars could be represented by one-dimensional elements (link, spring, truss) because experimental tests have proved that steel bars slip in their own direction (failure mode 2). Therefore, one-dimensional elements could simulate the response of the interface layer between concrete and steel reinforcement. However, 2- or 3-dimensional elements could be defined to the interface layer in a way that the stiffness of cohesive layer should be higher in comparison to mode 2, where there would be no slippage in modes 1 and 3. This later technique increases the time of the FE analysis.

Telford [22] proposed the most accepted model for both plane and deformed bars to implement the interface layer that account for ascending and softening parts. Since the deformed bars are now used for both stirrups and longitudinal bars, the following presents the model proposed by Telford [22] for bond-slip relationship between concrete and deformed steel bars (Figure 7):

$$\begin{aligned}
\tau &= \tau_{max}\left(\frac{s}{s_1}\right)^{\alpha} \text{ If}(s_0 \le s \le s_1),\\
\tau &= \tau_{max} \text{If}(s_1 \le s \le s_2),\\
\tau &= \tau_{max} - (\tau_{max} - \tau_f)\left(\frac{s - s_2}{s_3 - s_2}\right),\\
&\text{If } (s_2 \le s \le s_3),\\
\tau_{max} &= \tau_f \text{ If}(s_3 \le s),
\end{aligned} \quad (25)$$

where $\alpha = 0.4$, $s_1 = s_2 = 0.6$ mm, and $s_3 = 1$ mm.

$$\begin{aligned}
\tau_{max} &= 2.0 \times \sqrt{f_{ck}},\\
\tau_f &= 1.5 \times \tau_{max}.
\end{aligned} \quad (26)$$

4.12. Ratio of FRP, Stirrups, and Longitudinal Bars. The ratio of FRP composites, longitudinal tensile steel reinforcement, and transverse steel stirrups affects the shear resistance of EB-FRP strengthened RC beams. In addition, the ultimate load-carrying capacity of the beam depends on the complex interaction among these reinforcing elements. Therefore, more FE parametric studies are required to clarify these interactions and their underlying mechanisms to achieve an optimized design model for the shear resistance of a beam. FEA is a powerful and cost-effective tool to perform such studies compared to experimental tests. For longitudinal steel reinforcement, it has been shown that assuming a perfect bonding model can reduce the shear resistance of

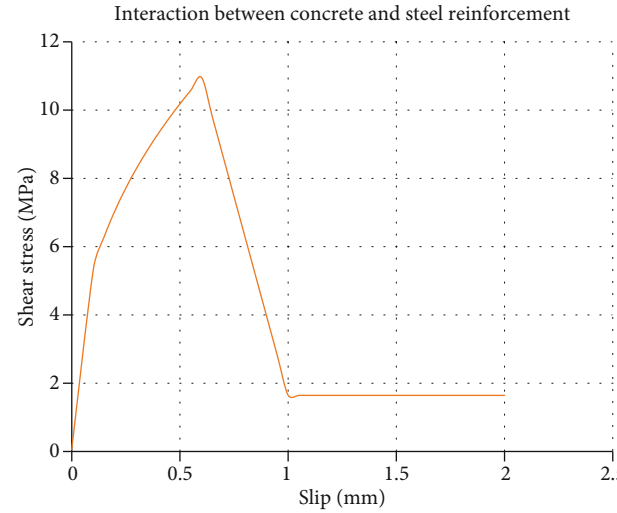

FIGURE 7: Telford [22] model for bond-slip relation between concrete-deformed bars ($f'_c = 30$ MPa).

specimens by reducing the shear contribution of EB-FRP in beams where the shear cracks are more distributed and inclined at a high angle with respect to the horizontal axis of the beam. Indeed, FRP laminates/fabrics crossed by shear cracks at a high angle are less solicited and result in less FRP contribution to shear resistance [3]. More than 100 beams were selected from the database to evaluate the interaction between longitudinal reinforcement and EB-FRP, as illustrated in Figures 8(a)–8(d). The figures reveal that the contribution of EB-FRP to shear resistance is reduced by increasing the amount of longitudinal tensile reinforcement, confirming the results reported by Chen et al. [3]. For steel stirrups, it has been demonstrated by Bousselham and Chaallal [15] that the higher the stiffness of the steel stirrups, the less is the EB-FRP contribution to shear resistance. Finally, previous investigations (FEA, experimental tests, and analytical models) have demonstrated that, given the EB-FRP propensity to debonding failure, increasing the stiffness and cross section of EB-FRP could increase the FRP contribution to resistance up to a threshold, beyond which no increase in FRP contribution would occur because it is limited by the effective bond length [9]. 138 (57.7%) of the 239 beams were subjected to FEA that evaluated the ratio of reinforcing components, of which only 33 (13.8%) were T-shaped, and 2 (less than 1%) were I-shaped cross sections (Figure 4). There is a need for more FE studies to develop a reliable closed-form model for calculating the respective contributions of these shapes to shear resistance.

4.13. Dimension of the Beam (Size Effect). The size effect is considered as a factor that can have a negative impact on the load-carrying capacity of RC beams. If all parameters are kept unchanged, the shear resistance of RC beams, particularly deep beams, will decrease as the beam's depth increases [23]. More than 100 specimens from the study database were considered to evaluate the relation between the beam depth and shear span-to-depth ratio versus normalized shear strength, as

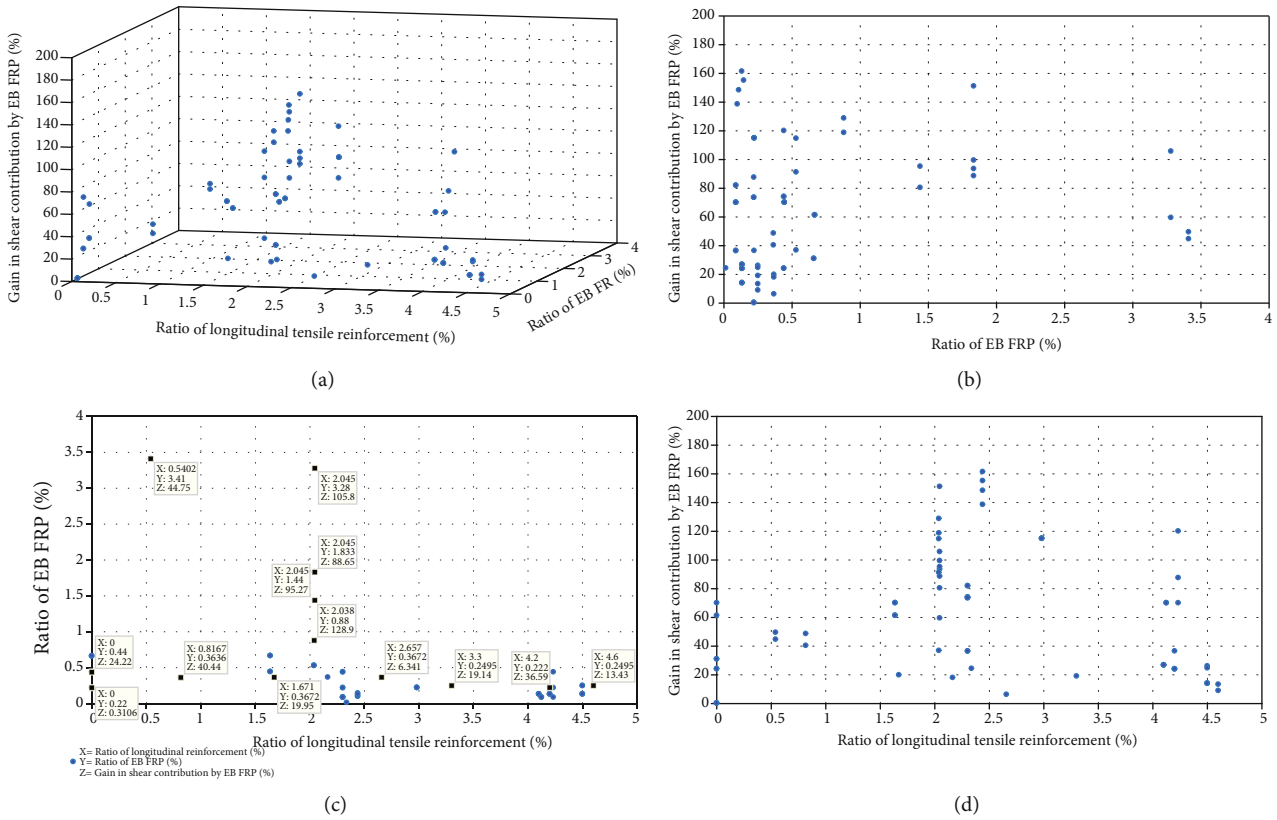

Figure 8: Interaction between longitudinal tensile reinforcement and EB-FRP versus shear gain contributions.

illustrated in Figures 9(a)–9(c). The figures reveal that, given the shear span-to-depth ratio (a/d), increasing the beam's depth (d) reduces the normalized shear strength of the RC beam strengthened in shear using EB-FRP, which confirms the results obtained by Benzeguir et al. [23]. The database shows that few studies have been performed on the size effect of shear-strengthened RC beams using EB-FRP. Two known theories related to the size effect are generally used: the Weibull theory and the theory based on fracture mechanics. The model proposed by Bazant and Planas [24] is the only closed-form model that considers this effect and can be expressed as:

$$\sigma_{Nu} = \frac{Bf_t'}{\sqrt{1 + D/D_0}}. \quad (27)$$

A complete parametric study on the size effect on EB-FRP RC beams was conducted by Benzeguir et al. [23], where five major factors influencing the size effect were evaluated: the shear-span-to depth ratio a/d, the aggregate size a_g, the ratio of longitudinal tension bars ρ_w, the ratio of steel stirrups ρ_s, and the concrete strength f'_c. Many numerical studies have been carried out on beams of different sizes. However, the aim of these numerical studies was not to evaluate the size effect in RC beams strengthened in shear using EB-FRP composites. 165 (69%) of the 239 beams in this study were analyzed by FEA to study the effect of beam dimension, of which 149 (62.3%) were rectangular, 14 (5.8%) were T-shaped, and 2 (less than 1%) were I-shaped cross sections (Figure 4).

5. Validation of Numerical FEA and Experimental Tests

The validation of over 200 specimens strengthened with different configurations (side-bonded, U-shaped, fully wrapped, EB with anchorage, ETS, NSM) and unstrengthened (control beams) is carried out to evaluate the accuracy of the FEA results in terms of ultimate load-carrying capacity of the specimens. Figure 10 shows the numerical versus experimental results for total strength achieved by all the specimens. The results reveal that the FE studies predicted the experimental tests with good agreement because the square of the Pearson product-moment correlation coefficient (R^2) was greater than 99% for all beams.

6. Synthesis, Results, and Recommendations

FEA provides a powerful tool that can replace experimental tests if accurate assumptions are provided to the software and the required in-depth knowledge is obtained regarding parameters that affect dynamic analysis, such as loading pattern (smoothing, stepping, or ramping), impact loading duration, amount of damping for EB-FRP RC beams, and finally time increment when performing nonlinear dynamic analysis. FEA of RC beams strengthened in flexure is well

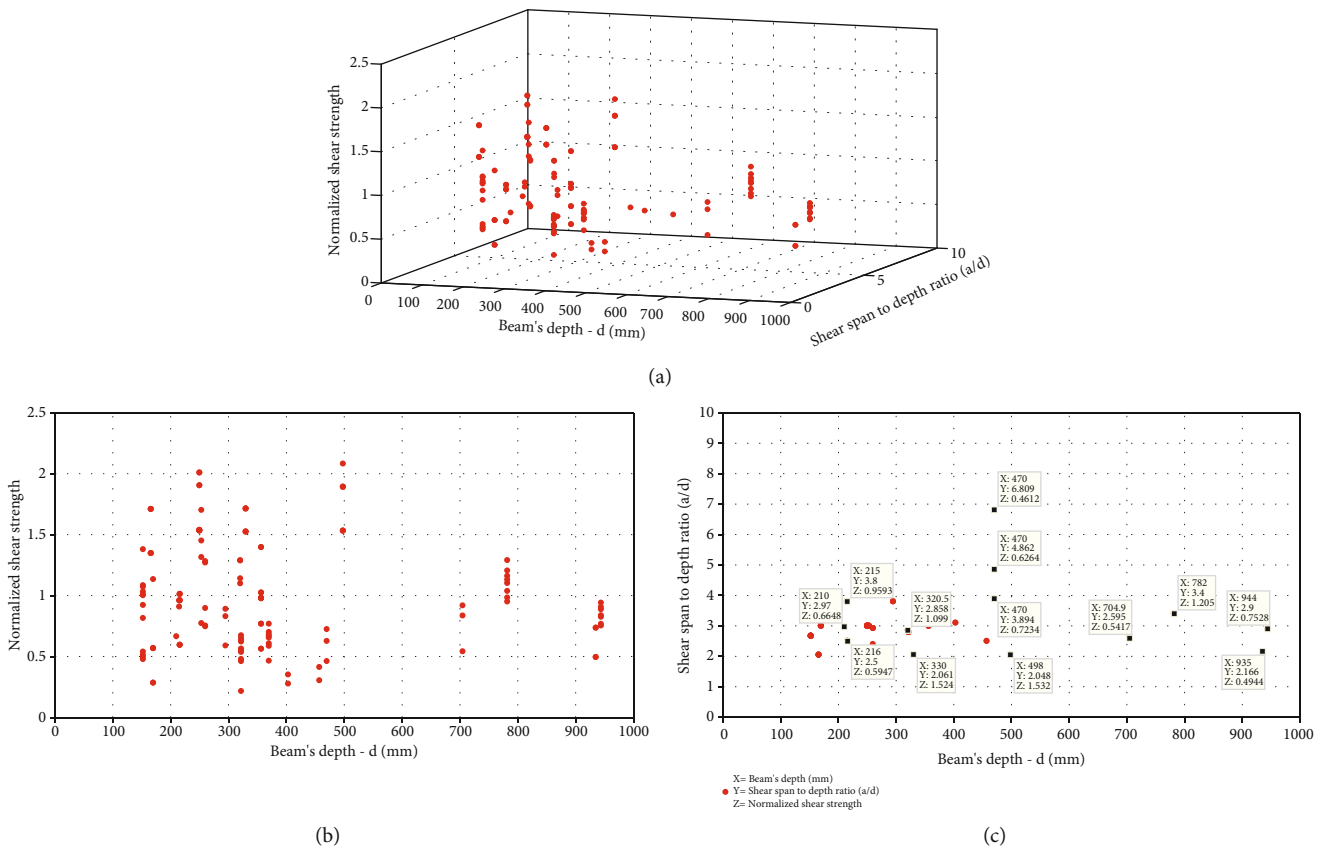

Figure 9: Effect of shear span-to-depth ratio on size effect versus normalized shear strength.

documented. This does not hold true for RC beams strengthened in shear using EB-FRP composites, where clearly there is a need for more research studies. Indeed, first, the brittle behavior of shear cracks in RC beams is still unpredictable and becomes even more complex when RC beams are strengthened in shear with EB-FRP because the type of EB strengthening affects the shear crack pattern. Second, interactions between the components of such strengthened beams have not been fully documented, and indirect interactions between the components and their effects on each other are still not fully understood. Third, selecting the right type of finite element for each component of these beams is of paramount importance and needs a theoretical and experimental understanding of the response of each material when used for shear strengthening.

From existing FE studies on EB-FRP RC beams, it is obvious that early studies assumed perfect bond-slip models for their specimens, and only 18.4% (44 beams) of all the FE studies considered bond-slip laws for both concrete-to-FRP and concrete-to-steel reinforcement interactions. This has led to incorrect results because Bousselham and Chaallal [15] proved that increasing the rigidity of steel stirrups results in a reduction of EB-FRP contribution to shear resistance. Therefore, defining appropriate bond-slip laws between all the various materials involved in a study must be a priority. Furthermore, Chen et al. [6] showed that there is an inverse interaction between internal and external reinforcement and that its effect should be considered in a closed-form model, suggesting a need for research on this phenomenon.

Because of the unpredictable nature of shear cracking, most international guidelines recommend a crack angle of 45°, which is obviously overestimated, but conservative. The crack shape functions presented by Lu et al. [7] are based on four simplified assumptions, leading to unrealistic stress and strain distributions for fibers intercepted by the shear crack. Moreover, from the data evaluated earlier, 35.1% (84 beams) of all FE studies considered the stress and strain distributions along the shear crack. In addition, the assumption of one main shear crack is to some extent unrealistic because experimental tests revealed more marginal distributed shear cracks that contributed to shorter effective bond length. Therefore, more research is needed to encompass the patterns and shapes of shear cracks for EB-FRP strengthened RC beams.

The smeared crack model in conjunction with the crack band model is an appropriate model for defining shear cracks in concrete. These should be considered alongside appropriate bond-slip laws between all components of EB-FRP RC beams to achieve an accurate simulation of the real specimen. It may be worth noting that, from the FE data already gathered, only 5% (12 beams) research studies have observed this phenomenon.

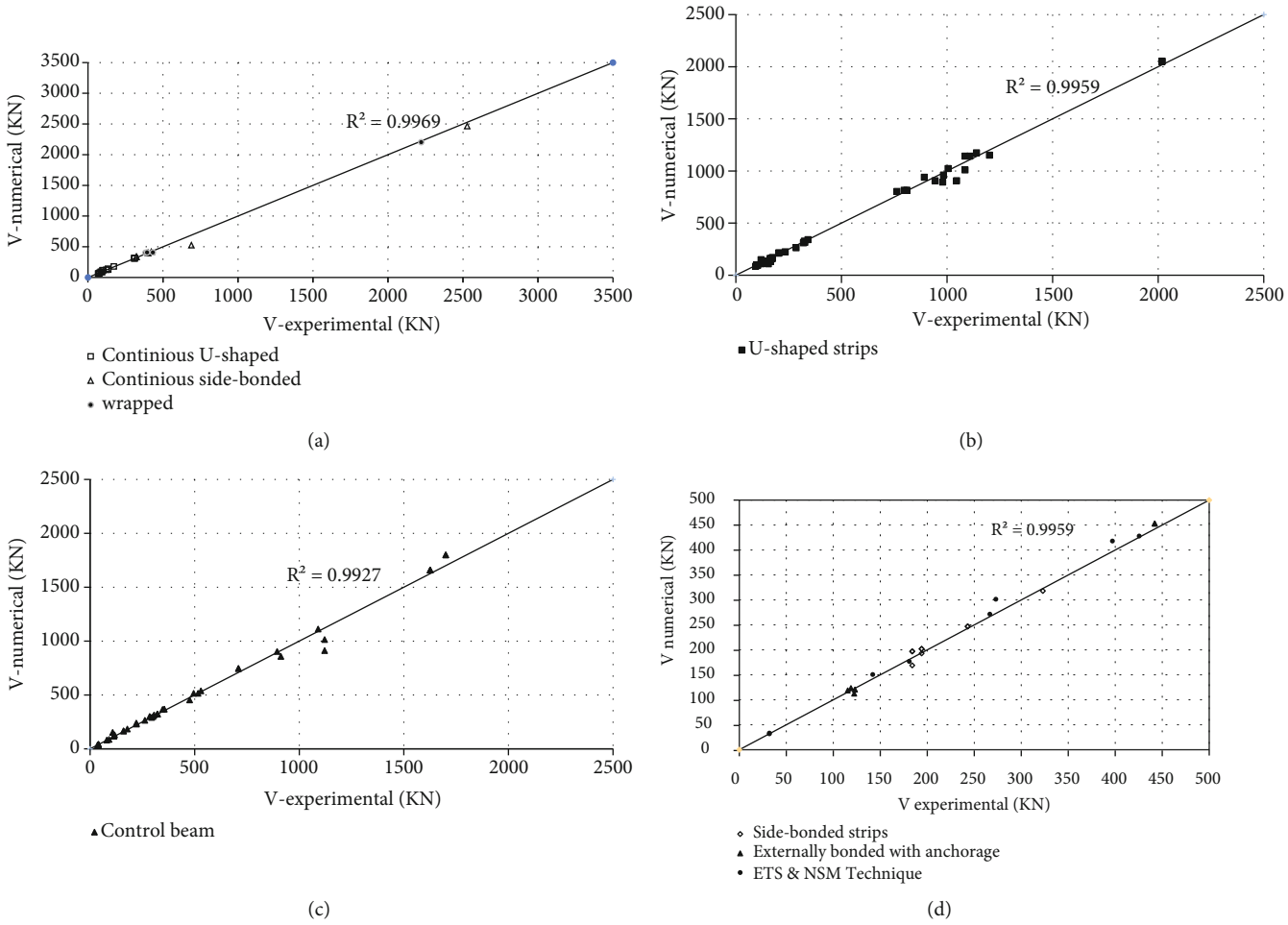

Figure 10: Numerical versus experimental ultimate load-carrying capacity of the specimens for (a) continuous U-shaped, continuous side-bonded, fully-wrapped; (b) U-shaped strips; (c) control beam; and (d) side-bonded strips, EB with anchorage, ETS, and NSM methods.

7. Conclusions

This study has concentrated on the evaluation of many factors affecting the accuracy of simulating RC beams strengthened in shear with EB-FRP and of parameters studied by researchers through FEA. To that end, an extensive database consisting of over 200 FE specimens validated by experimental tests was gathered and evaluated in this study. The most relevant features drawn from the FEA and the studied parameters were as follows:

(i) To achieve an accurate simulation reflecting the behavior of the real beam, the parameters and elements introduced in FEA should represent the real response of each component. Essential building blocks of FEA include the smeared crack model alongside the crack band model and the bond-slip law to describe concrete-to-FRP and concrete-to-steel reinforcement interactions, and dynamic analysis in which parameters such as the structure-damping ratio, the time increment, the crack pattern, and the loading duration are well characterized. Less than 6% of all FE studies addressed these parameters, and none of them described the implementation details

(ii) After FEA is performed on RC beams strengthened in shear with EB-FRP, the study parameters obtained from the output to develop the analytical model should be extracted precisely, and their complex effects on each other should be carefully examined. The angle of the shear crack in concrete, the interaction between components of specimens, the inverse interaction between internal and external reinforcements, the shape of the shear crack, the stress and strain distributions along the shear cracks, the size effect, and the type of FRP configuration are some of these important interacting parameters

(iii) The ultimate load-carrying capacity of a specimen is not the only good indication for evaluating the overall specimen response. FEA is a powerful and useful tool for evaluating other important response indicators, considering all the beam components during

the process of loading. Therefore, based on the built database, studies are needed to consider the influencing parameters required to develop a reliable closed-form model to calculate with confidence the EB-FRP contribution to shear resistance

(iv) FEA can capture the real behavior of a beam, including details that can be important to the research community, such as the number and angle of shear cracks and the stress distribution along the shear cracks and fibers

(v) By drawing comparisons between variations in the ratio of EB-FRP and in the ratio of steel stirrups, it is obvious that for each ratio of steel stirrups, there exists only one peak for the ratio of EB-FRP corresponding to the maximum gain due to FRP. This inverse interaction should be considered for optimal design

(vi) When drawing comparisons between FRP contributions to shear resistance in RC beams strengthened in shear using EB-FRP, the negative impact of size effect should be included in any final closed-form model

Data Availability

All data, models, and code generated or used during the study appear in the submitted article.

Conflicts of Interest

The authors declare that they have no conflicts of interest.

Acknowledgments

Financial support from the Natural Sciences and Engineering Research Council of Canada (NSERC) and from the Fonds de recherche du Québec - Nature et Technologies (FRQ-NT) through operating grants is gratefully acknowledged.

References

[1] J. Lubliner, J. Oliver, S. Oller, and E. Oñate, "A plastic-damage model for concrete," *International Journal of Solids and Structures*, vol. 25, no. 3, pp. 299–326, 1989.

[2] J. Lee and G. L. Fenves, "Plastic-damage model for cyclic loading of concrete structures," *Journal of Engineering Mechanics*, vol. 124, no. 8, pp. 892–900, 1998.

[3] G. M. Chen, J. F. Chen, and J. G. Teng, "On the finite element modelling of RC beams shear-strengthened with FRP," *Construction and Building Materials*, vol. 32, pp. 13–26, 2012.

[4] A. Bousselham and O. Chaallal, "Effect of transverse steel and shear span on the performance of RC beams strengthened in shear with CFRP," *Composites Part B: Engineering*, vol. 37, no. 1, pp. 37–46, 2006.

[5] Comité Euro-International du Béton, *CEB-FIP Model Code 1990: Design Code*, Thomas Telford, London. UK, 1993.

[6] G. M. Chen, J. G. Teng, J. F. Chen, and O. A. Rosenboom, "Interaction between steel stirrups and shear-strengthening FRP strips in RC beams," *Journal of Composites for Construction*, vol. 14, no. 5, pp. 498–509, 2010.

[7] X. Z. Lu, J. F. Chen, L. P. Ye, J. G. Teng, and J. M. Rotter, "RC beams shear-strengthened with FRP: stress distributions in the FRP reinforcement," *Construction and Building Materials*, vol. 23, no. 4, pp. 1544–1554, 2009.

[8] J. F. Chen and J. G. Teng, "Shear capacity of fiber-reinforced polymer-strengthened reinforced concrete beams: fiber reinforced polymer rupture," *Journal of Structural Engineering*, vol. 129, no. 5, pp. 615–625, 2003.

[9] G. Chen, *Behaviour and Strength of RC Beams Shear-Strengthened with Externally Bonded FRP Reinforcement*, The Hong Kong Polytechnic University, 2010.

[10] A. Mofidi and O. Chaallal, "Shear strengthening of RC beams with EB FRP: influencing factors and conceptual debonding model," *Journal of Composites for Construction*, vol. 15, no. 1, pp. 62–74, 2010.

[11] U. Neubauer and F. S. Rostasy, "Design aspects of concrete structures strengthened with externally bonded CFRP-plates," in *PROCEEDINGS OF THE SEVENTH INTERNATIONAL CONFERENCE ON STRUCTURAL FAULTS AND REPAIR, 8 JULY 1997. VOLUME 2: CONCRETE AND COMPOSITES*, 199746 Cluny Gardens Edinburgh, United Kingdom.

[12] J.-F. Chen and J. G. Teng, "Shear capacity of FRP-strengthened RC beams: FRP debonding," *Construction and Building Materials*, vol. 17, no. 1, pp. 27–41, 2003.

[13] S. A. Mirza, M. G. JG, and M. Hatzinikolas, "Statistical descriptions of strength of concrete," *Journal of the Structural Division*, vol. 105, no. 6, pp. 1021–1037, 1979.

[14] J. G. Teng, J. F. Chen, S. T. Smith, and L. Lam, *FRP: strengthened RC structures*, Wiley, 2002.

[15] A. Bousselham and O. Chaallal, "Shear strengthening reinforced concrete beams with fiber-reinforced polymer: assessment of influencing parameters and required research," *Structural Journal*, vol. 101, no. 2, pp. 219–227, 2004.

[16] X. Z. Lu, J. G. Teng, L. P. Ye, and J. J. Jiang, "Bond–slip models for FRP sheets/plates bonded to concrete," *Engineering Structures*, vol. 27, no. 6, pp. 920–937, 2005.

[17] K. Nakaba, T. Kanakubo, T. Furuta, and H. Yoshizawa, "Bond behavior between fiber-reinforced polymer laminates and concrete," *Structural Journal*, vol. 98, no. 3, pp. 359–367, 2001.

[18] G. Monti, M. Renzelli, and P. Luciani, "FRP Adhesion in Uncracked and Cracked Concrete Zones," in *Fibre-Reinforced Polymer Reinforcement for Concrete Structures*, vol. 2, pp. 183–192, World Scientific, 2003.

[19] M. Savoia, B. Ferracuti, and C. Mazzotti, "Non Linear Bond-Slip Law for FRP-Concrete Interface," in *Fibre-Reinforced Polymer Reinforcement for Concrete Structures*, vol. 2, pp. 163–172, World Scientific, 2003.

[20] J. G. Dai and T. Ueda, "Local Bond Stress Slip Relations for FRP Sheets-Concrete Interfaces," in *Fibre-Reinforced Polymer Reinforcement for Concrete Structures*, vol. 2, pp. 143–152, World Scientific, 2003.

[21] T. Ueda, J. G. Dai, and Y. Sato, "A Nonlinear Bond Stress-Slip Relationship for FRP Sheet-Concrete Interface," in *The International Symposium on Latest Achievement of Technology and Research on Retrofitting Concrete Structures*, vol. 113, pp. 107–112, Japan Concrete Institute, 2003.

[22] Thomas Telford Publishing, *CEB-FIP Model Code 1990: Design Code*, Thomas Telford Publishing, Lausanne, Switzerland, 1993.

[23] Z. E. Benzeguir, G. El-Saikaly, and O. Chaallal, "Size effect in shear of conventional and shear-strengthened RC beams with EB-FRP: state of knowledge and research needs," *Global Journal of Advanced Engineering Technologies and Sciences*, vol. 4, no. 11, pp. 1–23, 2017.

[24] Z. P. Bazant and J. Planas, *Fracture and Size Effect in Concrete and Other Quasibrittle Materials*, CRC press, 1997.

[25] V. N. Kaliakin, M. J. Chajes, and T. F. Januszka, "Analysis of concrete beams reinforced with externally bonded woven composite fabrics," *Composites Part B: Engineering*, vol. 27, no. 3-4, pp. 235–244, 1996.

[26] M. Arduini, A. Di Tommaso, and A. Nanni, "Brittle failure in FRP plate and sheet bonded beams," *ACI Structural Journal*, vol. 94, no. 4, pp. 363–370, 1997.

[27] M. Amir, "Analytical study of reinforced concrete beams strengthened with web-bonded fiber reinforced plastic plates or fabrics," *ACI Structural Journal*, vol. 95, no. 3, pp. 12–16, 1998.

[28] F. J. Vecchio and F. Bucci, "Analysis of repaired reinforced concrete structures," *Journal of Structural Engineering*, vol. 125, no. 6, pp. 644–652, 1999.

[29] T. K. Lee, R. S. Al-Mahaidi, and G. R. Taplin, "Non-linear finite element modelling of shear-damaged concrete T-beams repaired with CFRP laminates," in *In ACUN-2 Int. Composites Conference*, pp. 253–258, University of New South Wales, 2000.

[30] K. Damian, M. Thomas, Y. Solomon, C. Kasidit, and P. Tanarat, *Finite Element Modeling of Reinforced Concrete Structures Strengthened with FRP Laminates*, Report for Oregon Department of Transportation, Salem, Oregon, 2001.

[31] R. S. Y. Wong and F. J. Vecchio, "Towards modeling of reinforced concrete members with externally bonded fiber-reinforced polymer composites," *ACI Structural Journal*, vol. 100, no. 1, pp. 47–55, 2003.

[32] R. Santhakumar, E. Chandrasekaran, and R. Dhanaraj, "Analysis of retrofitted reinforced concrete shear beams using carbon fiber composites," *Electronic Journal of Structural Engineering*, vol. 4, no. 1, pp. 66–74, 2004.

[33] I. Elyasian, N. Abdoli, and H. R. Rounagh, *Evaluation of Parameters Effective in FRP Shear Strengthening of RC Beams Using FE Method*, ASIAN JOURNAL OF CIVIL ENGINEERING (BUILDING AND HOUSING), 2006.

[34] O. F. A. Otoom, S. T. Smith, and S. J. Foster, *Finite Element Modelling of FRP Shear Strengthened RC Beams*, ePublications, 2006.

[35] Z. Qu, X. Z. Lu, L. P. Ye, J. F. Chen, and J. M. Rotter, "Numerical modeling of FRP shear strengthened RC beams using compression field theory," in *Proceedings, third international conference on FRP composites in civil engineering (CICE 2006)*, pp. 391–394, Miami, Florida, USA, 2006.

[36] S. T. Smith, O. Otoom, and S. J. Foster, *Finite Element Modelling of RC Beams Strengthened in Shear with FRP Composites*, ePublications, 2006.

[37] A. Godat, K. W. Neale, and P. Labossière, "Numerical modeling of FRP shear-strengthened reinforced concrete beams," *Journal of Composites for Construction*, vol. 11, no. 6, pp. 640–649, 2007.

[38] A. Godat, P. Labossière, and K. W. Neale, "Numerical prediction of shear crack angles for FRP shear-strengthened concrete beams," in *4th International conference on FRP composites in civil engineering (CICE2008)*, p. 6, Zurich, Switzerland, 2008.

[39] H.-K. Lee, S.-K. Ha, and M. Afzal, "Finite element analysis of shear-deficient RC beams strengthened with CFRP strips/sheets," *Structural Engineering and Mechanics*, vol. 30, no. 2, pp. 247–261, 2008.

[40] A. Godat, Z. Qu, X. Z. Lu, P. Labossiere, L. P. Ye, and K. W. Neale, "Size effects for reinforced concrete beams strengthened in shear with CFRP strips," *Journal of Composites for Construction*, vol. 14, no. 3, pp. 260–271, 2010.

[41] Y.-M. You, A. Ayoub, and A. Belarbi, "Three-dimensional nonlinear finite-element analysis of prestressed concrete beams strengthened in shear with FRP composites," *Journal of Composites for Construction*, vol. 15, no. 6, pp. 896–907, 2011.

[42] R. A. Hawileh, J. A. Abdalla, M. H. Tanarslan, and M. Z. Naser, "Modeling of nonlinear cyclic response of shear-deficient RC T-beams strengthened with side bonded CFRP fabric strips," *Computers and Concrete*, vol. 8, no. 3, pp. 193–206, 2011.

[43] R. A. Hawileh, T. A. El-Maaddawy, and M. Z. Naser, "Nonlinear finite element modeling of concrete deep beams with openings strengthened with externally-bonded composites," *Materials & Design*, vol. 42, pp. 378–387, 2012.

[44] S. Dirar, J. M. Lees, and C. Morley, "Phased nonlinear finite-element analysis of precracked RC T-beams repaired in shear with CFRP sheets," *Journal of Composites for Construction*, vol. 17, no. 4, pp. 476–487, 2012.

[45] A. Godat, P. Labossière, and K. W. Neale, "Numerical investigation of the parameters influencing the behaviour of FRP shear-strengthened beams," *Construction and Building Materials*, vol. 32, pp. 90–98, 2012.

[46] A. Godat, P. Labossière, K. W. Neale, and O. Chaallal, "Behavior of RC members strengthened in shear with EB FRP: assessment of models and FE simulation approaches," *Computers & Structures*, vol. 92, pp. 269–282, 2012.

[47] S. Imperatore, D. Lavorato, C. Nuti, S. Santini, and L. Sguerri, "Numerical modeling of existing RC beams strengthened in shear with FRP U-sheets," in *Proceedings of the 6th International Conference on FRP Composites in Civil Engineering—CICE2012*, pp. 13–15, Rome, Italy, 2012.

[48] A. M. Sayed, X. Wang, and W. Zhishen, "Modeling of shear capacity of RC beams strengthened with FRP sheets based on FE simulation," *Journal of Composites for Construction*, vol. 17, no. 5, pp. 687–701, 2013.

[49] G. C. Manos, M. Theofanous, and K. Katakalos, "Numerical simulation of the shear behaviour of reinforced concrete rectangular beam specimens with or without FRP-strip shear reinforcement," *Advances in Engineering Software*, vol. 67, pp. 47–56, 2014.

[50] M. Qapo, S. Dirar, J. Yang, and M. Z. E. B. Elshafie, "Nonlinear finite element modelling and parametric study of CFRP shear-strengthened prestressed concrete girders," *Construction and Building Materials*, vol. 76, pp. 245–255, 2015.

[51] E. O. Ibars, D. Ferreira, A. M. Bernat, and J. M. B. García, "Numerical analysis of reinforced concrete beams strengthened in shear by externally bonded (EB) fibre reinforced polymer (FRP) sheets," *Hormigón y acero*, vol. 69, no. 285, pp. 113–120, 2018.

[52] M. S. al Jawahery, M. E. Gulsan, H. M. Albegmprli, I. A. H. Mansoori, and A. Cevik, "Experimental investigation of rehabilitated RC haunched beams via CFRP with 3D-FE modeling analysis," *Engineering Structures*, vol. 196, article 109301, 2019.

[53] L. Jin, H. Xia, J. Xuan-ang, and D. Xiuli, "Size effect on shear failure of CFRP-strengthened concrete beams without web

reinforcement: meso-scale simulation and formulation," *Composite Structures*, vol. 236, article 111895, 2020.

[54] R. Hawileh, M. Tanarslan, M. Naser, and J. A. Abdalla, "Experimental and numerical investigation on the performance of shear deficient RC beams strengthened with NSM GFRP reinforcement under cyclic loading," *Dimensions*, vol. 7, no. 7, p. 7, 2011.

[55] A. Godat, O. Chaallal, and K. W. Neale, "Nonlinear finite element models for the embedded through-section FRP shear-strengthening method," *Computers & Structures*, vol. 119, pp. 12–22, 2013.

[56] M. Qapo, S. Dirar, and Y. Jemaa, "Finite element parametric study of reinforced concrete beams shear-strengthened with embedded FRP bars," *Composite Structures*, vol. 149, pp. 93–105, 2016.

[57] R. A. Hawileh, J. A. Abdalla, and M. Z. Naser, "Modeling the shear strength of concrete beams reinforced with CFRP bars under unsymmetrical loading," *Mechanics of Advanced Materials and Structures*, vol. 26, no. 15, pp. 1290–1297, 2019.

[58] A. Shomali, D. Mostofinejad, and M. R. Esfahani, "Effective strain of CFRP in RC beams strengthened in shear with NSM reinforcements," *structures*, vol. 23, pp. 635–645, 2020.